



1 **Contrasting seasonal changes in total and intense precipitation in the** 2 **European Alps from 1903 to 2010**

3
4 Ménégoz, Martin¹, Valla, Evgenia¹, Jourdain, Nicolas. C.¹, Blanchet, Juliette¹, Beaumet, Julien¹,
5 Wilhelm, Bruno¹, Gallée, Hubert¹, Fettweis, Xavier², Morin, Samuel³, Anquetin, Sandrine¹

6
7 1 CNRS, Université Grenoble Alpes, Institut de Géosciences de l'Environnement (IGE), 38000 Grenoble, France

8 2 F.R.S.-FNRS, Laboratory of Climatology, Department of Geography, University of Liège, 4000 Liège, Belgium

9 3 Univ. Grenoble Alpes, Université de Toulouse, Météo-France, CNRS, CNRM, Centre d'Études de la Neige, 38000
10 Grenoble, France

11 **Abstract**

12
13 Changes of precipitation over the European Alps are investigated with the regional climate
14 model MAR applied with a 7-km resolution over the period 1903-2010 using the reanalysis
15 ERA-20C as forcing. A comparison with several observational datasets demonstrates that the
16 model is able to reproduce the climatology as well as both the inter-annual variability and the
17 seasonal cycle of precipitation over the European Alps. The relatively high resolution allows to
18 estimate precipitation at high elevations. The vertical gradient of precipitation simulated by
19 MAR over the European Alps reaches 33% km⁻¹ (1.21 mm.day⁻¹.km⁻¹) in summer and 38%
20 km⁻¹ (1.15 mm.day⁻¹.km⁻¹) in winter, on average over 1971-2008 and shows a large spatial
21 variability. A significant (p-value<0.05) increase in mean winter precipitation is simulated in the
22 North Western Alps over 1903-2010, with changes typically reaching 20 to 40% per century.
23 This increase is mainly explained by a stronger simple daily intensity index (SDII) and is
24 associated with less frequent but longer wet spells. A general drying is found in summer over the
25 same period, exceeding 20 to 30% per century in the Western plains and 40 to 50% per century
26 in the Southern plains surrounding the Alps, but remaining much smaller (<10%) and not
27 significant above 1500 m.asl. Below this level, the summer drying is explained by a reduction of
28 the number of wet days, reaching 20% per century over the Northwestern part of the Alps and
29 30-50% per century in the Southern part of the Alps. It is associated to shorter although more
30 frequent wet spells. Maximum daily precipitation index (Rx1day) takes its highest values in
31 autumn in both the Western and the Eastern parts of the Southern Alps, locally reaching 50 to 70
32 mm.day⁻¹ on average over 1903-2010. Centennial maxima up to 250 to 300 mm.day⁻¹ are
33 simulated in the Southern Alps, in France and Italy, as well as in the Ticino valley in
34 Switzerland. Over 1903-2010, seasonal Rx1day shows a general and significant increase at the
35 annual timescale and also during the four seasons, reaching local values between 20% and 40%
36 per century over large parts of the Alps and the Apennines. Trends of Rx1day are significant (p-
37 value<0.05) only when considering long time series, typically 50 to 80 years depending on the
38 area considered. Some of these trends are nonetheless significant when computed over 1970-
39 2010, suggesting a recent acceleration of the increase in extreme precipitation, whereas earlier
40 periods with strong precipitation also occurred, in particular during the 1950s/1960s.

41



42 1. Introduction

43

44 The European Alps are often considered as the “water tower” of continental Europe (Beniston et
45 al., 2018), hosting the headwaters of several major European rivers, such as the Rhine, the
46 Danube, the Po, and the Rhône Rivers. Similar to other mountain regions of the world, this stems
47 from both enhanced precipitation rates compared to surrounding lowlands, and by the specific
48 role played by glaciers and the mountain snow cover in regulating the local and regional
49 hydrological cycle (Wanner et al., 1997, Viviroli et al., 2008; 2019). The high population density
50 and the presence of strong slopes makes these areas particularly prone to natural hazards such as
51 landslides, floods and avalanches, which are strongly connected to meteorological conditions
52 (e.g. Beniston M., 2006; Evin et al., 2019). There is widespread evidence from scientific studies
53 addressing past and future climate conditions, that significant atmospheric warming, largely due
54 to anthropogenic forcing (Hock et al., in press), has been and is projected to occur in the
55 European Alps. This warming is estimated to 1.2°C per century over the 20th century (Auer et
56 al., 2007), which is twice as large as global rates (Brunetti et al., 2009; Gobiet et al., 2014).
57 Precipitation changes are more difficult to detect because of (i) the difficulty to observe and
58 simulate this variable over mountainous areas, (ii) the stronger influence of internal variability
59 and (iii) the spatial heterogeneity peculiar to complex topography areas.

60

61 The longest time series of observed precipitation in the European Alps are available in
62 Switzerland and Italy, with station data that have been homogenized over the last 100 to 150
63 years (i.e starting from 1900 and even before; Schmidli et al., 2002; Brugnara and Maugeri,
64 2019). Such a long record is useful to investigate precipitation changes, but station data need to
65 be considered carefully, because the spatio-temporal heterogeneity of the data availability might
66 be a cause of spurious trends (e.g. Masson and Frei, 2016). Interpolation of station data can be
67 used to produce gridded products, commonly used to investigate climate variability. For
68 example, SAFRAN (Durand et al., 2009) and SPAZM (Gottardi et al., 2009) are two reanalyses
69 covering the French Alps, HISTALP (Auer et al., 2007) and EURO4M (Isotta et al., 2014) are a
70 reconstruction of the climate of the European Alps, and E-OBS is a dataset commonly used for
71 model verification over Europe (Cornes et al., 2018). General Circulation Models (GCMs) are
72 also widely used to investigate climate change processes and trends. However, their coarse
73 resolution precludes accurate simulations of small scale processes typical of mountainous areas,
74 such as those inducing the spatial heterogeneity of precipitation and snow cover. It is therefore
75 difficult to study the Alpine climate variability with GCMs (Zubler et al., 2015). Due to their
76 finer resolution (~25 to 1 km) and their more detailed parametrization for physical processes
77 (e.g. precipitation microphysics, surface snow scheme), that can be developed and tuned
78 specifically considering regional geographical features, Regional Climate Models (RCMs) are
79 more adapted to simulate the mountainous climate and can be used to dynamically downscale
80 global climate model or global reanalyses. They have been widely used to simulate the climate in
81 mountainous areas, and in particular temperature (Smiatek et al., 2009), daily and sub-daily
82 precipitation events (Torma et al., 2014; Pieri et al., 2015), precipitation trends (Giorgi et al.,
83 2016) and snow cover (Steger et al., 2013). A fine resolution is critical to simulate correctly



84 precipitation. Increasing the resolution from 0.44° to 0.11° , Fantini et al. (2018) demonstrated
85 that a RCM better captures the spatial pattern and the seasonal cycle of precipitation as well as
86 its daily intensities and statistics. The improvement of the model performances allows currently
87 to run RCMs at high resolution, typically 1 to 5 km, in non-hydrostatic configurations, resolving
88 the convective processes, and allowing an accurate description of the snow cover in mountainous
89 areas (e.g. Ban et al., 2014, 2015; Luthi et al., 2019). Such configuration is however challenging
90 to run over more than one to two decades due to computational costs.

91

92 Internal climate variability in the North Atlantic basin induces large seasonal to multi-decadal
93 variability of precipitation over Europe (Dell'Aquila et al., 2018). Using gridded observations,
94 Efthymiadis et al. (2007) and Brunetti et al. (2006) described the spatiotemporal distribution of
95 precipitation in the European Alps, highlighting higher interannual variability in the Southern
96 compared to the Northern Alpine areas. Seasonally, higher interannual variability in winter and
97 autumn compared to other seasons has also been observed in the European Alps (Brunetti et al,
98 2009; Bartolini et al, 2009). At daily to interannual time scales, the variability of precipitation
99 across the Alps is influenced by large-scale atmospheric circulations and particularly by the
100 North Atlantic Oscillation (NAO). A general picture is that a positive phase of the NAO induces
101 higher precipitation rates over the Northern Alps and lower ones over the Southern Alps, and
102 vice versa for negative phases of the NAO. This general view nonetheless hides important
103 heterogeneities, as local conditions can drive strong variations of local temperature, wind and
104 moisture transport that may amplify or mitigate synoptical atmospheric patterns (Keiler et al.,
105 2010). In addition, the NAO-precipitation relationship over the Alps is not stationary over the
106 last two centuries (Brunetti et al., 2006). At decadal timescales, the Atlantic Multidecadal
107 Variability (AMV) affects the precipitation rates over the Alps as suggested by Brugnara and
108 Maugeri (2019) using correlations with station data. However, the compensating effects of the
109 thermodynamical and dynamical signals of the AMV on the surrounding continents might induce
110 a strong nonlinearity between the AMV and the precipitation rates in Europe (Qasmi et al.,
111 2017).

112

113 Over the last decades, precipitation rates have been declining for any period of the year in the
114 mediterranean area (Giorgi et al., 2008; Mariotti et al., 2015), a signal partly attributed to
115 anthropogenic forcings (Hoerling et al., 2012) and associated with a significant surface drying
116 (Douville et al., 2017). Precipitation trends during the last century are more contrasted over the
117 Alps, with a decrease in the Southeastern Alps consistent with the drying of the mediterranean
118 area (Schmidli et al., 2002; Auer et al., 2007; Brugnara and Maugeri, 2019) and an increase in
119 the annual precipitation in the North Western Alps, mainly driven by a positive and significant
120 trend in winter and at high elevation (Masson and Frei, 2014; 2016). Napoli et al. (2019)
121 suggested that the contrasted trends of precipitation between high mountains and lowlands over
122 the last decades is explained by the aerosol forcing that cools the atmosphere mainly at low
123 elevations since the air quality is better at high elevations. The contrasted seasonal trends in
124 precipitation needs to be considered separately since their sign can be different from one season
125 to another one. In addition, precipitation trends emerge from the natural variability only when



126 considering long time series, typically one century (Schmidli et al., 2002). This result is
127 consistent with previous studies claiming that precipitation rates did not show any significant
128 trend in the Alps when considering shorter periods, as found in Durand et al. (2009) in the
129 French Alps over the period 1958-2002.

130

131 Dry spells did not show any clear tendency over the last century in the Alps (Schmidli and Frei,
132 2005; Brugnara and Maugeri, 2019), whereas the length of dry episodes increased in the
133 Mediterranean area (Kuglitsch et al. 2010). On the other hand, Schmidli and Frei (2005)
134 highlighted contrasting seasonal trends of the wet spell duration over the Swiss Alps, with a
135 lengthening in winter and a shortening in summer. Using 104 rain gauge stations in Switzerland,
136 Schmidli and Frei (2005) found an increase of the high quantiles of precipitation by 10% to 30%
137 over 1901-2000, a result evidencing an increase of extreme precipitation in this area, that they
138 relate to global climate change. Considering the annual maximum of daily precipitation
139 (Rx1day), which is often used as an indicator of extreme precipitation, Brugnara and Maugeri
140 (2019) found a similar signal in Switzerland over 1890–2017, whereas they could not highlight a
141 clear trend of extreme precipitation in Northern Italy. Using a convection-resolving RCM at 2.2
142 km resolution over the European Alps, Ban et al., (2015) confirmed the significant decrease in
143 mean summer precipitation related to global warming, and also find an increase in extreme
144 precipitation events that asymptotically intensifies following the Clausius-Clapeyron
145 relationship. Using model data over the last 400 years and over the 21st century, Brönniman et
146 al. (2018) pointed out that heavy precipitation change should thermodynamically increase with
147 temperature increase at the daily timescale, following the Clausius-Clapeyron relationship.
148 However, they evidenced a limitation of the available moisture in the atmosphere at the seasonal
149 timescale, a signal that limits the increase of heavy precipitation during the summer, and induces
150 a shift of heavy precipitation events from late summer to early summer and early autumn.

151

152 RCMs are limited-area models that can be forced laterally by atmospheric reanalysis, often
153 available only for the last decades, such as the ECMWF reanalyses ERA40 (1958-2002, Uppala
154 et al., 2004), ERA-Interim (1979-2019, Dee et al., 2011) and ERA5 (1950 onward, Hersbach and
155 Dee, 2016). Recent reanalysis products available for the whole 20th century (e.g. ERA20C,
156 1900-2010; Poli et al., 2016) now offer the possibility to apply RCMs over longer periods
157 although such a reanalysis, assimilating few data, is less reliable than reanalysis built on the
158 satellite era. Most of the observational and modeling data used to investigate climate change in
159 the European Alps generally do not combine a daily resolution, a centennial availability and a
160 fine spatial resolution, precluding investigations of changes in mean and extreme precipitation.
161 This strongly limits the possibility to detect precipitation trends, especially when considering the
162 large internal variability that may overwhelm long-term trends. In this study, daily precipitation
163 variability and changes in the European Alps (referred to as the Alps in the rest of the text) are
164 investigated over the period 1903-2010, using observational datasets as well as the regional
165 climate MAR model applied with a resolution of 7 km and driven by the ERA20C reanalysis.
166 The material and methods, including a description of the model MAR and different observational
167 datasets are described in Section 2. The model outputs are compared with several observational



168 datasets in Section 3. Seasonal and annual trends of precipitation indices are estimated over
169 1903-2010 in section 4. A discussion associated to the conclusions is presented in Section 5.

170

171 **2. Material and methods**

172

173 **2.1 The MAR model**

174

175 In this section we provide a succinct description of the atmospheric regional model MAR
176 (<http://mar.cnrs.fr/index.php>), developed at ULiège (Belgium) and IGE (Grenoble). A more
177 detailed description can be found in Gallée and Schayes (1994), Gallée (1995) and Gallée et al.
178 (2001, 2005). MAR is a hydrostatic primitive equation model with a vertical coordinate defined
179 as sigma coordinates. The radiative transfer through the atmosphere uses the radiative scheme of
180 the ECMWF reanalysis (Morcrette, 2002). MAR includes a detailed scheme of clouds
181 microphysics with six prognostic equations for specific humidity, cloud droplets concentration,
182 cloud ice crystals (concentration and number), concentration of precipitating snow particles and
183 rain drops. The convective adjustment is parameterised according to Bechtold et al. (2001).
184 MAR is coupled to the one-dimensional land surface scheme SISVAT (Soil Ice Snow
185 Vegetation Atmosphere Transfer, De Ridder and Schayes, 1997; Gallée et al., 2001) that
186 includes a snow multi-layer scheme (Brun et al., 1992) including prognostic equations for
187 temperature, mass, water content and snow properties (dendricity, sphericity and size) as well as
188 an ice module (Lefebvre et al., 2003). As pointed out in Messenger et al. (2006), the physics of
189 MAR can be adjusted to the region of interest and can be used with relatively high resolutions
190 (40 to 7 km, finer resolutions would not be possible when using the hydrostatic configuration).
191 MAR is a limited area model that offers the big advantage to be able to be forced by most of
192 reanalyses (including ERA-20C) or CMIP5/CMIP6 global model outputs. MAR has been first
193 designed for polar regions (Gallée, 1995), i.e. Antarctica (e.g., Gallée et al., 1996; Naithani, J. et
194 al., 2002; Gallée et al., 2013, Amory et al. 2015; Agosta et al. 2019) and Greenland (Fettweis et
195 al., 2017). It has also been applied over tropical regions (Messenger et al., 2004) to investigate the
196 precipitation variability (Gallée, 2004). MAR has also been used to simulate the climate at
197 midlatitudes (e.g. Wyard et al., 2016), and in particular to study changes of precipitation over
198 Europe (Doutreloup et al., 2019). It has been applied over various mountainous areas, e.g.
199 Himalaya (Ménégoz et al., 2013), Svalbard (Lang et al., 2015), Kerguelen archipelago (Favier et
200 al., 2016; Verfaillie et al., 2019) and Antarctic peninsula (Datta et al., 2017).

201

202 **2.2 MAR configuration**

203

204 We used the version 3.9.0 of the MAR model, which is an open source code available at
205 mar.cnrs.fr/. Here, the model has been applied over the European Alps with a domain that
206 extends from 43.5°N to 48°N and 5°E to 13°E and includes 140 x 90 grid points, at 7 km
207 horizontal resolution. This configuration is based on 24 levels in the atmosphere, 7 levels in the
208 soil, and the snow cover is described with a number of layers varying from 1 to 20. Here, MAR
209 is laterally forced with the 6-hourly outputs of the ERA-20C reanalysis and its dynamical and



210 physical schemes are applied with a time step of 60s. ERA-20C is one of the first reanalyses
211 available from 1900 to 2010, assimilating surface pressure and near-surface winds over the
212 ocean and forced by SST reconstructions (Poli et al., 2016). By assimilating a limited number of
213 variables corresponding to those available relatively homogeneously over 1900-2010, the
214 ERA20-C reanalysis is expected to be homogeneous over this period, with a limited risk of
215 including spurious trend. However this reanalysis is probably less accurate than other products
216 assimilating also humidity and temperature in the free troposphere, a weakness that could induce
217 model biases also in regional experiments as evidenced by Fettweis et al. (2017) over Greenland.
218 MAR has already been successfully tested with the ERA20-C reanalysis as boundary conditions
219 over Europe (Wyard et al., 2017; 2018). After a spin-up of 2 years, the model in general and the
220 surface component in particular are supposed to reach an equilibrium. Therefore, the first years
221 have been excluded from this analysis that hence focuses on the period 1903-2010.

222

223 **2.3 Observational datasets**

224

225 Observational data sets are used in this study for two objectives: first, a comparison between the
226 model outputs and the different precipitation datasets have been conducted over 1971-2008, a
227 period for which all the datasets are available (Section 3). Second, an analysis of the trends of
228 several precipitation indices is described using the MAR experiments and the MeteoSwiss
229 station data available since the beginning of the 20th century (Section 4). In addition to the
230 MeteoSwiss station data, the following datasets have been considered:

231

232 **HISTALP**

233 The HISTALP (“Historical instrumental climatological surface time series”) is the first long-
234 term database of meteorological data collected in the European Alps, initiated in the 1990s (Auer
235 and Bohm, 1994) and completed later on (Auer, et al., 2007). This dataset is available for air
236 temperature at 2 meters, surface pressure, precipitation, sunshine duration and cloudiness
237 through two different configurations: a first one including monthly homogenized time series of
238 local measurements, with the first observations available from 1760 for temperature and 1800 for
239 precipitation and a second one provided as a 1° gridded version. The gridded version, used in our
240 study, is available from 1800 to 2014.

241

242 **EURO4M-APGD**

243 The Alpine Precipitation Grid Dataset (EURO4M-APGD, Isotta et al., 2014) is a 5kmx5km grid
244 analysis of daily precipitation, extending over the European Alps and covering the period 1971-
245 2008. It is based on rain-gauge networks, encompassing more than 8500 stations from Austria,
246 Croatia, France, Germany, Italy, Slovenia and Switzerland. This dataset was developed in the
247 framework of the European Reanalysis and Observations for Monitoring (EURO4M) initiative
248 and is simply named EURO4M thereafter.

249

250



251 **E-OBS**

252 E-OBS is provided by the ECA&D project under the Copernicus Climate Change Service (van
253 den Besselaar et al., 2011). It is a daily gridded dataset over Europe for temperature and
254 precipitation, produced from interpolation of local measurements at two available resolutions:
255 0.25° and 0.1° (the highest resolution is used in this study). It is available from 1950 and updated
256 each year, and is commonly used for model evaluation (e.g. Guillod et al., 2017). The version 19
257 of E-OBS offers an estimate of the uncertainty related to the interpolation of local observations
258 by providing a 100-member ensemble for each variable (Cornes et al., 2018).

259
260 **SAFRAN**

261 The SAFRAN reanalysis combines large scale reanalyses and forecasts with in-situ
262 meteorological observations, including precipitation, in order to provide a reanalysis of
263 meteorological conditions in the French Alps, at the scale of massifs with a typical surface area
264 of 1000 km² within which meteorological conditions are assumed to be homogenous but vary
265 with elevation by steps of 300 m (Durand et al., 2009). Hence this reanalysis does not use a
266 regular grid but focuses on the elevation dependency of meteorological conditions.

267
268 **SPAZM**

269 The SPAZM dataset is a gridded product at a 1km resolution for minimum and maximum daily
270 2m temperature and daily precipitation in the French Alps, available over the period 1948-2009
271 and based on the interpolation of a dense network of rain gauges and temperature sensors from
272 Météo-France and the French Company for Electricity (EDF; Gottardi et al., 2009). This dataset
273 is provided with calibration parameters allowing to reproduce the stream flow observed in the
274 Rhône valley with a hydrological model. These parameters are useful to correct the snowfall
275 rates that are often underestimated in rain gauge measurements. The solid and liquid
276 precipitation has been computed by considering 100% of solid precipitation below 0°C and
277 100% of liquid precipitation above 2°C, considering daily temperature. A linear relationship for
278 the ratio liquid/solid precipitation has been applied between 0°C and 2°C. Following the
279 calibration suggested by Picouet (2012), we applied a correction factor for solid precipitation of
280 1.5 in the Northern Alps and 1.3 elsewhere. The Northern Alps are defined here as the areas
281 located north of Grenoble city (45.1885° N) and higher than 1000m asl. This apparently-
282 arbitrary values have been developed and evaluated in the context of hydrological studies
283 (Gouttevin et al., 2017).

284
285 **2.4 Statistical analysis and indices**

286
287 Mean and trends for the precipitation indices described in Table 1 are considered in this study,
288 most of them selected from those recommended by the World Meteorological Organization
289 (Peterson et al., 2001; http://etccdi.pacificclimate.org/list_27_indices.shtml). When comparing
290 MAR outputs with observational datasets based on a higher resolution (EURO4M, SPAZM),
291 these ones are linearly interpolated onto the MAR grid. The gridded data are based on regular
292 grids, except the SAFRAN data that is provided with a georeferenced polygon describing the



293 location of each massif. Correlation and Root Mean Square Error (RMSE) are computed to
294 investigate the differences between datasets. The linear trends are computed with a linear least-
295 square regression and a two-sided p-value is computed to test if the trends are significantly
296 different from zero (Wald test with a t-distribution of the test statistic). Mean values and
297 normalized trends (in percentage of the averaged values) are computed annually and seasonally
298 for the precipitation rates and indices in the following sections. The seasons are computed by
299 averaging indices over December-January-February (DJF) for winter, March-April-May (MAM)
300 for spring, June-July-August (JJA) for summer, and September-October-November (SON) for
301 autumn.

302 **3. Climatology of the MAR experiment and the observational datasets**

303 **3.1 Spatial differences**

304 The Total Precipitation amount (TP) averaged over 1971-2008 simulated with MAR is shown in
305 Figure 1a, with annual mean ranging between 300 and 3000 mm. In a general way, TP is
306 stronger in the Northern than in the Southern Alps as expected due to the drier Mediterranean
307 climate in the South. A comparison between the MAR experiment and the EURO4M reanalysis
308 (Figure 1b) shows a good consistency between these two datasets in the lowlands (i.e. below
309 500m asl), with positive or negative differences barely exceeding 20% in these areas. Above
310 1500m, this difference is much higher with precipitation rates 40 to 80% higher in the MAR
311 experiment than in the EURO4M dataset. Such a difference is significant with respect to the
312 interannual standard deviation of precipitation that generally does not exceed 30% over the
313 domain of application of MAR (Figure A1). The comparison between MAR and SPAZM
314 (Figure 1c) shows similar differences in the lowlands as with EURO4M (~20%), but a better
315 agreement at high elevation, with differences barely exceeding 40%. Correlation pattern between
316 MAR and EURO4M is 0.59 and reaches 0.63 between MAR and SPAZM, suggesting a slightly
317 better spatial consistency between these last two products. The precipitation rates estimated from
318 SPAZM above 1500m asl are also higher in comparison with those provided by EURO4M
319 (Figure 1d, differences ranging between 20% to 80%). As snowfall rates in SPAZM have been
320 adjusted to fit the hydrological balance over the French Alps, this comparison suggests that the
321 high precipitation rates simulated with MAR above 1500m asl may be realistic. Overall, TP
322 simulated with MAR is relatively similar to TP estimated from SPAZM and show stronger
323 values with respect to EURO4M data over the Alps.

324 **3.2 Vertical gradients**

325 Vertical gradients of TP simulated with MAR are evidenced in Figure 2 (as yearly averages,
326 considering both wet and dry days), including also a comparison with the SAFRAN reanalysis
327 and the MeteoSwiss station data. In the MAR experiment, TP varies from 2 to 4 mm day⁻¹ at
328 500m asl and from 3 to 5 mm day⁻¹ at 2500m asl in the Southern Alps, and from 2 to 4 mm day⁻¹
329 at 500m asl and from 3 to 6 mm day⁻¹ at 2500m asl in the Northern French Alps. The vertical
330 gradient estimated from the SAFRAN dataset is smaller than those simulated by MAR. The large
331 spread in the scatter plots of Figures 2a-b is explained by the spatial variability of the vertical



332 gradient of precipitation, which is stronger in MAR than in SAFRAN. Based on a comparison
333 with high resolution numerical weather forecast model and glacier mass balance in mountain
334 glaciers in the French Alps, it has been shown that SAFRAN most likely underestimates high
335 elevation winter precipitation (above 2000m asl), which lends credence to the higher gradients
336 simulated by MAR (Vionnet et al., 2019). MAR data are compared to the MeteoSwiss station
337 data in Figure 2c-d. A difference between the two datasets in terms of vertical gradients is found
338 both in winter (14% km⁻¹ for the local observations vs 43% km⁻¹ in the MAR data) and in
339 summer (12% km⁻¹ for the local observations vs 20% km⁻¹ in the MAR data). These seasonally
340 contrasted differences suggest a possible underestimation of the precipitation rates estimated
341 from rain gauge measurements in relation with snowfall undercatch issues (Kochendorfer et al.,
342 2017). However, the differences found in summer, i.e. a period with reduced snowfall rates, also
343 suggests an overestimation of the precipitation rates at high elevation in the MAR experiment.
344 Overall, it is difficult to accurately quantify the model biases at high elevation areas because of
345 the scarceness of the observational data above 2000m asl whereas a large number of the MAR
346 grid cells reaches an elevation ranging between 2000m asl and 3000m asl with a spatial
347 resolution of 7km (Figure 2c-d). The vertical gradient of precipitation simulated by MAR over
348 the entire domain of application reaches 38% km⁻¹ (1.15 mm.day⁻¹.km⁻¹) in winter and 33%
349 km⁻¹ (1.21 mm.day⁻¹.km⁻¹) in summer (Figure 2e-f). Overall, the spatial patterns shown in
350 Figure 2g-h for the MAR experiment and the MeteoSwiss station data suggest that MAR is able
351 to reproduce the seasonal variations of precipitation rates, with large (small) values in summer in
352 the Northeastern (Southwestern) Alps and an opposite pattern in winter.

353 **3.3 Interannual variability and seasonal cycle**

354 The temporal evolution of precipitation and its seasonal cycle over the period 1971-2008 is
355 shown in Figure 3 for three sub-regions defined as the Southern Alps (SA, 43.5°N to 45.5°N and
356 5°E to 7.5°E), the North Western Alps (NWA, 45.5°N to 47°N and 5°E to 7.5°E) and the
357 Northeastern Alps (NEA, 45.5°N to 48°N and 7.5°E to 13°E), corresponding respectively to the
358 orange, blue and purple boxes in Figure 1a. These boxes have been defined according to the data
359 availability of the products used for comparisons as well as regional climatological conditions:
360 SA is largely affected by the Mediterranean dry conditions, NWA precipitations rates are mainly
361 related to Western low pressure systems, whereas NEA is more typical of a continental climate,
362 with wetter conditions in summer than in winter. Over 1971-2008, precipitation rates estimated
363 from the different datasets (EURO4M, SPAZM, E-OBS, HISTALP) show similar features. They
364 range between 2 and 4 mm day⁻¹ in SA and take higher values in NWA and NEA, varying
365 between 3 and 5 mm day⁻¹. Table 2 includes the interannual correlations between the different
366 datasets, that takes values above 0.8, except for HISTALP that correlates neither with EURO4M
367 nor with MAR. The correlations between MAR and the observational datasets range between
368 0.84 and 0.89, whereas the correlations among these different datasets systematically exceeds
369 0.9, even reaching 0.99 and 0.97 for EURO4M versus SPAZM in SA and NWA. Such high
370 correlation is probably due to the rain gauge network used to produce these gridded datasets that
371 is partially common between the two products. Overall these correlation values suggest a correct
372 interannual variability in the MAR experiment, but less realistic than those estimated from the



373 other observational datasets (except HISTALP). The model bias could be related to both model
374 deficiencies and uncertainties in the ERA20C reanalysis used as boundary conditions. The
375 difference between the MAR experiment and the observational products is similar in all the
376 datasets, with a RMSE ranging between 0.26 and 1.14. RSME computed with HISTALP are
377 comparable to the other ones, evidencing that HISTALP is able to provide an estimation of
378 precipitation similar to the other products, even if the interannual variability is poorly
379 reproduced in this dataset compared to the other ones (low correlation). No clear regional and
380 data-dependant specificity in terms of RMSE is discernable in Table 2. It is worth noting that the
381 uncertainty related to data interpolation in E-OBS (orange dashed lines) encompasses the time
382 series corresponding to the other datasets. Such a large uncertainty is probably related to the low
383 number of observations assimilated in E-OBS over the Alps in comparison with the large
384 number of meteorological stations used to build EURO4M and SPAZM. It also points out the
385 large uncertainty of such gridded products in mountainous areas. MAR is closer to SPAZM and
386 EURO4M (smaller RMSE) than to HISTALP and E-OBS (higher RMSE), a finding giving
387 confidence in the realism of the MAR simulation. The different datasets show specific seasonal
388 cycles of precipitation (Figure 3, bottom), with two maximum values in spring and autumn in SA
389 (Mediterranean climate), one maximum value in summer in NEA (continental climate) and a
390 mix between these two regimes over NWA. Overall, the consistency between the different
391 datasets is better in SA and NEA than over NWA, where more discrepancies among the datasets
392 have been found. The comparison between model experiments and observational datasets gives
393 confidence in the precipitation rates simulated with the MAR model forced here by ERA-20C.
394 Longer simulations are therefore considered in the next section to investigate potential trends
395 over the last century.

396 **4. Precipitation trends in the Alps over 1903-2010**

397 **4.1 Mean annual and seasonal precipitation**

398 No significant trend in precipitation rates is identified on average when considering the three
399 Alpine sub-regions shown in Figure 3, a finding that could be explained by the shortness of the
400 time series. The seasonal trends of mean precipitation (STP) are investigated now over a longer
401 period, by considering in Figure 4 the MAR experiment (shaded) and the MeteoSwiss station
402 data (dotted) over 1903-2010. The MeteoSwiss data is used here because it is available over the
403 period covered by the MAR experiment (i.e. from 1903). Trends are contrasted both seasonally
404 and altitudinally. In winter, there is a general positive trend in precipitation over the Alps (up to
405 40% per century), contrasting with a drying simulated in the surrounding plains (~10% per
406 century), both in the Po plain and in the Rhône valley (Figure 4a). In winter, the MAR
407 experiment is consistent with the local observations showing an increase in precipitation over
408 Switzerland, except in the southern part of this country, where some stations show a drying
409 trend. However, when masking the non significant trends ($p\text{-value} > 0.05$, Figure 4c), only the
410 positive trends of precipitation remain over the Alpine mountains, with values ranging between
411 20 and 40% per century in the Northern French Alps and in the Southwestern Switzerland, at an
412 elevation generally higher than 1500m asl. The MeteoSwiss data shows a significant increase in



413 precipitation at stations located further north in Switzerland, with a magnitude similar to the
414 model values. In summer, a general drying is simulated over the whole model domain (Figure
415 4b), with values exceeding 40 to 50% per century in the Po and the Rhône valleys. This signal is
416 much less pronounced in the alpine areas located above 1500m asl, where the signal is generally
417 not significant (Figure 4d). The drying is less pronounced over Switzerland in comparison with
418 the Southern Alps. Considering Figure 4b, a drying and even a slight increase in precipitation
419 (<10% per century) is found in the station data over the mountains of Southern Switzerland,
420 whereas a drying is observed in the north of the country (10% to 20% per century). The summer
421 trends locally observed in Switzerland are however barely significant (Figure 4d). Spring and
422 autumn trends show intermediate patterns, with a drying pronounced in the plains, and a slight
423 moistening in the mountainous areas (Figure 4e-f). The trends simulated and observed during
424 spring and autumn are however smaller and barely significant, except in the Po plain where a
425 drying is simulated by MAR and in the North of Switzerland where a significant moistening is
426 significant at some stations (Figure 4g-h).

427 **4.2 Wet spells**

428 Changes of the wet spell features are highlighted in Figure 5, showing the centennial summer
429 and winter trends of WD (Figure 5a-b), SDII (Figure 5c-d), MNWS (Figure 5g-h) and MWSD
430 (Figure 5e-f). In winter and over the Alps, the slight increase in WD, ranging between 0 and
431 10% per century, is slightly contributing to the increase in the STP (Figure 5a), but this one is
432 mainly explained by an increase in SDII by 10 to 30% per century (Figure 5c). These changes
433 are associated with an increase in the MWSD by 10 to 20% per century (Figure 5e). Finally, the
434 winter trend in the MNWS shows a different pattern from the previous ones (Figure 5g), with a
435 consistent decrease over the Northern Alps and in particular over Switzerland, ranging between
436 10 and 20% per century in both model and observational data. These changes suggest that the
437 precipitation increase found in winter over the Alpine mountains is related to longer, more
438 intense and less frequent wet spells. The agreement between the model and the observations is
439 relatively good in winter. In summer, a large part of the drying is explained by a reduction of
440 WD, reaching 10 to 20% in the north-western flank of the Alps, and exceeding 40 to 50% per
441 century in all the Southeastern Alps (Figure 5b). The SDII shows smaller changes during this
442 season (Figure 5d), that can be either positive or negative and barely exceeding 10% per century.
443 A general decrease of MWSD is also found in summer (Figure 5f), especially pronounced over
444 the Southeastern flank of the Alps and in the Po plain, a signal consistent between the model and
445 the observations over Switzerland. Finally, the model shows a general increase in MNWS
446 (Figure 5h) in summer, which is particularly strong over the Southeastern flank of the Alps. Over
447 Switzerland, this signal is small and not consistent with the observations that show a minor
448 reduction of MNWS. Overall, these results suggest that the decrease of the mean precipitation
449 rates over the Alps in summer is explained by a dramatic reduction of WD, with shorter and
450 more frequent wet spells without any clear change of SDII.

451



452 **4.3 Extreme precipitation**

453 The means and the trends of extreme precipitation rates are described by considering Rx1day
454 seasonally (Figure 6) and annually (Figure 7). Extreme precipitation shows contrasted seasonal
455 and spatial climatological patterns (Figure 6a-c-e-g). In winter and spring, it takes higher values
456 over the Southern Alps (both in France and in Italy) than in the Northern Alps (Figure 6a-c). In
457 summer, extreme values are smaller in the Western Alps than in the Eastern Alps. The most
458 intense events are found in autumn, in both the Western and the Eastern parts of the Southern
459 Alps, with mean Rx1day ranging between 50 and 70 mm day⁻¹ in many areas (Figure 6g). Over
460 Switzerland, the climatological pattern of Rx1day is consistent between the model and the
461 observations, except for some local exceptions. In contrast with the trends of mean precipitation
462 (Figure 4), there is a general increase in Rx1day (Figure 6b-d-f-h) that occurs over the four
463 seasons and both in the plains and in the mountainous areas. The trend in the seasonal Rx1day
464 over the period 1903-2010 takes values between 0 and 40% per century, and generally ranges
465 between 20% and 40% per century over the Alpine mountain range. Such increase in
466 percentages, suggests strong changes of local extreme, in particular in the regions where strong
467 events are frequent in autumn (50 to 70 mm day⁻¹, Figure 6g). The magnitude of the change in
468 Rx1day is similar between the model and the observations, but the MeteoSwiss station data show
469 more heterogeneous spatial trends, with some locations where the trends can be small and even
470 slightly negative. The mean increase in Rx1day over the model domain reaches 10, 10, 6 and
471 13% per century, respectively in winter, spring, summer and fall, confirming a constant increase
472 in Rx1day for all the seasons.

473 The climatological mean of the annual Rx1day (Figure 7a) is dominated by the seasonal Rx1day
474 computed in autumn that shows a similar pattern (Figure 6g). Centennial Rx1day (Figure 7b,
475 maximum Rx1day computed over 1903-2010) shows a pattern similar to the annual average of
476 Rx1day. The strongest centennial events are found in the Southern Alps, in France and Italy, as
477 well as in the Ticino valley in Switzerland, with extreme values locally reaching 250 to 300 mm
478 day⁻¹. The annual trends are inspected in Figure 7c, highlighting a general increase in extreme
479 precipitation. The significance of this trend is described in Figure 7d, where non-significant
480 trends (p-value>0.05) are masked. The annual samples considered here are obviously larger than
481 the seasonal samples, allowing to detect more efficiently significant trends. In that case, a good
482 consistency is found between the model and the MeteoSwiss station, both of them showing only
483 positive trends, ranging between 20 and 40% per century, and covering large parts of the Alps
484 and the Apennines.

485 **4.4 Statistical significance of the trends**

486 The large interannual to decadal variability of the climate in the Europe-North-Atlantic region,
487 in relation with internal climate variability, makes precipitation trends challenging to detect in
488 the Alps. When considering time series over 1971-2008, i.e. a relatively short period, there is no
489 clear tendency of the mean precipitation over the Alps (Figure 3). By computing trends from the
490 beginning of the 20th century, winter increase and summer decrease of mean precipitation



491 emerge from interannual to decadal variability over large areas (Figure 4 c-d). Similarly, the
492 positive trends of the annual Rx1day are significant (p -value <0.05) over large areas of the Alps,
493 in particular where the trends are positive and strong (i.e. $>10\%$ per century), whereas all the
494 negative and small trends in both the model data at the MeteoSwiss station data are not
495 significant (Figure 7d). Figure 7e illustrates the trend of the annual Rx1day, considering the
496 average of the MeteoSwiss data (purple), the model data integrated over Switzerland (blue) and
497 the model data integrated over the whole model domain (red). In agreement with the patterns
498 shown in Figure 7c-d, the mean trend in the annual Rx1day in Figure 7 is positive for both the
499 model outputs and the observations, reaching 9.43, 8.74 and 8.40 mm day⁻¹ per century
500 respectively for the MeteoSwiss data, the model over Switzerland and the model over the whole
501 domain. The vertical bars in Figure 7e show the length of the time series required to identify a
502 significant trend over the period 1903-2010, starting from 2010 and going back into the past.
503 Time series has to be considered from 1961, 1932 and 1942 until 2010 to get significant trends
504 (p -value <0.05) for the MeteoSwiss data, the model integrated over Switzerland and the model
505 integrated over the whole domain respectively, which correspond to length of ~ 50 to ~ 80 years.
506 We nonetheless see that shorter time series can lead to significant signals as evidenced in Figure
507 7f showing the p -value computed to estimate the significant level of the trend. The three curves
508 reach values below 0.05 during the years 1960-1970, highlighting significant trends of Rx1day
509 over 1960-2010 for the observations and over 1970-2010 for the model data.

510 **5. Discussions and conclusions**

511

512 Previous work highlighted a temperature increase in the Alps over the last century, associated
513 with an increase in precipitation over the Northern Alps in winter and a drying in summer
514 (Schmidli et al., 2002; Auer et al., 2007; Masson and Frei, 2014; 2016; Brugnara and Maugeri,
515 2019). The detailed features of climate change over the Alps remain however partly unknown, in
516 particular because of the lack of observational data at high elevation, and observational issues
517 with snow precipitation. In addition, the large internal variability of the climate system,
518 especially pronounced in Europe, may overwhelm long-term trends that remain challenging to
519 detect. Here, the MAR model has been used at a 7km resolution over the Alps, over the period
520 1900-2010 laterally forced with the ERA-20C reanalysis. A comparison with several datasets
521 (EURO4M, SPAZM, SAFRAN, E-OBS, HISTALP and local MeteoSwiss data) demonstrates
522 that the model is able to reproduce the climatological precipitation rates as well as both the
523 interannual variability and the seasonal cycle of precipitation over the Alps. The high resolution
524 used in the MAR experiment allowed a relatively correct representation of the topography, with
525 a large number of grid cells covering elevation between 2000m and 3500m, corresponding to
526 areas with few available observations. The vertical gradient of precipitation in the Alps is
527 estimated to 33% km⁻¹ (1.21 mm.day⁻¹.km⁻¹) in summer and 38% km⁻¹ (1.15 mm.day⁻¹.km⁻¹)
528 in winter, with values stronger in the Northern Alps than in the Southern Alps. The spatial
529 variability of this vertical gradient is large, being affected by the local climate conditions.

530

531 The model experiment confirms an increase in precipitation during the winter over the North
532 Western Alps, above 500m asl and significant and more pronounced above 1500m asl, with local



533 values of 20% to 30% per century over the period 1903-2010. This increase in precipitation is
534 related to stratiform precipitation, mainly explained by more intense precipitation during wet
535 days, and it is associated to longer albeit less frequent wet spells, a result consistent with
536 Schmidli and Frei (2005) over Switzerland. The model reproduces the general drying that
537 occurred in summer during the same period, exceeding 40% to 50% per century in the lowlands,
538 whereas it is much smaller (<10% per century) and not significant above 1500m asl. This drying
539 is not related to a decrease of the intensity of precipitation, but it is explained by a dramatic
540 reduction of the number of wet days, with shorter and more frequent wet spells. It is consistent
541 with previous work suggesting that the Alpine region appears as an exception in a drying region,
542 where local convective precipitation increases locally, in relation to surface warming and
543 sufficient moisture available in the soil at high-elevation areas (Giorgi et al., 2016).

544

545 The model reproduces the observed climatological patterns of the seasonal maximum
546 precipitation, and in particular the large values occurring in the Southern Alps in autumn,
547 exceeding 50 and even 70 mm day⁻¹ on average over the period 1903-2010. Centennial events
548 reaching 250 to 300 mm day⁻¹ are simulated in the Southern Alps, both in France and in Italy, as
549 well as in the Ticino valley. The seasonal maximum of precipitation shows a general increase
550 over this period and present during the four seasons, reaching values between 20% and 40% per
551 century in the Alps. An increase of strong precipitation has been evidenced in previous studies
552 over the European Alps in relation with higher temperature and moisture rates in the atmosphere
553 following the Clausius-Clapeyron relationship (e.g. Ban et al., 2015). However, this increase
554 might be modulated by the availability of moisture in the low troposphere and at the surface. The
555 drying of the surface may act as a positive feedback enhancing warming signals, that has been
556 identified as one of the causes of the Mediterranean amplification (Brogli et al., 2019).
557 Bronnimann et al. (2018) suggested a limited increase in Rx1day during the summer in the Alps
558 due to moisture limitation, pointing out a shift of this index typically observed at the end of the
559 summer toward early summer and early autumn. Here, the MAR experiment shows an increase
560 of Rx1day both annually and for all seasons, suggesting sufficient moisture available at the
561 surface and in the low troposphere over 1903-2010 in the model experiment. This difference
562 with Bronnimann et al. (2018) could be explained by a relatively high resolution (7km) in our
563 model configuration as well as specific physical parameterisations. Nevertheless, the MAR
564 experiment evidenced a significant increase in the Rx1day only in mountainous areas whereas no
565 significant signal is not found in the lowlands. This result is consistent with Brugnara et al.
566 (2019) who observed an increase in the Rx1day in the mountain areas of Switzerland, where
567 enough moisture would be available, whereas the drying occurring in the Southern flank of the
568 Italian Alps may prevent any increase in Rx1day.

569

570 In the MAR experiments, the trends of the seasonal maxima of precipitation integrated over the
571 Alps are significant (p-value<0.05) only when considering long time series, typically 50 to 80
572 years depending on the area considered. Some of these trends are nonetheless significant when
573 computed over recent decades, from the 1960s/1970s to the 2000s. This suggests a recent
574 acceleration of the increase in extreme precipitation, whereas earlier periods with strong



575 precipitation also occurred, in particular during the 1950s/1960s. These ones could be explained
576 by internal climate variability and/or the non-linear response of the climate system to
577 anthropogenic greenhouse gases and aerosols. In particular, the cooling related to aerosol
578 forcing, which peaked during the 1970s/1980s (Koch et al., 2011) over Europe could have
579 masked the warming related to greenhouse gases, and temporarily prevented changes of extreme
580 precipitation. Further model investigations should be conducted to disentangle the variability of
581 the Alpine climate related to internal variability and external forcings. This research is needed to
582 anticipate possibly strong precipitation changes in the Alps under the accelerating global climate
583 change.

584

585 **Data availability:**

- 586 • MAR is accessible at <https://gitlab.com/Mar-Group>, and documented at <http://mar.cnrs.fr/>
- 587 • The outputs of the MAR experiments will be uploaded to a public server (EUDAT) if the
588 paper is accepted and before publication.
- 589 • The scripts used in this study will be put on github if the paper is accepted.
- 590 • Alpine Precipitation Grid Dataset (EURO4M-APGD), Version 1, is available on-line at
591 DOI:10.18751/Climate/Griddata/APGD/1.0
- 592 • ECAD can be downloaded at <https://www.ecad.eu/download/ensembles/ensembles.php>
- 593 • SAFRAN data are available upon request to s2m.reanalysis@meteo.fr. Work is in progress to
594 release the data set on a public repository.
- 595 • The SPAZM dataset has been provided by EDF and Météo-France for this research. It could
596 be made available to other researchers under a specific research agreement. Requests should
597 be sent to dtg-demandedonnees-hydro@edf.fr

598

599 **Author contributions:** All authors contributed to design the study. XF, MM and JB ran MAR
600 experiments and produced the figures. MM wrote the manuscript and other authors contributed
601 with suggested changes and comments.

602

603 **Competing interests:** The authors declare no competing interests.

604

605 **Acknowledgements:** As part of the project CDP TRAJECTORIES, this work is funded by the
606 French National Research Agency in the framework of the " Investissements d'avenir" program
607 (ANR-15-IDEX-02). The authors thank the ERASMUS+ program and the VATEX project
608 founded under the program Labex OSUG@2020 (ANR10 LABX56). The author thank the
609 providers of observational datasets: MeteoSwiss, the federal office for meteorology and
610 climatology, for providing the data station over Switzerland as well as the EURO4M-APGD
611 dataset; the HISTALP group (<http://www.zamg.ac.at/histalp>); Électricité De France (EDF) for
612 providing the SPAZM dataset; the E-OBS dataset from the EU-FP6 project UERRA
613 (<http://www.uerra.eu>) and the data providers in the ECA&D project (<https://www.ecad.eu>). The
614 authors thank the "Institut du Développement et des ressources en Informatique" (IDRIS,
615 CNRS) and the GRICAD project (<https://gricad.univ-grenoble-alpes.fr/>) for providing computer
616 time for the simulations presented in this paper. The Figures have been produced with the python
617 package basemap (<https://matplotlib.org/basemap/>).



618 **Tables:**

619

Index	Unit	Description
TP	mm year-1	Total precipitation amount per year
STP	mm day-1	Total precipitation amount, including wet and dry days, seasonal or annual
WD	days	Number of wet days (≥ 1 mm)
SDII	mm day-1	Simple daily intensity (TP/WD)
Rx1day	mm day-1	Maximum daily precipitation, seasonal or annual
MNWS	no unit	Mean number of wet spells per season
MWSD	days	Mean wet spell duration, averaged over a season (WD/MNWS)

620

621

622

623

Table 1: Annual and seasonal precipitation indices analysed in this study. Precipitation is the sum of solid and liquid precipitation.

	Southern Alps (SA)	Northwestern Alps (NWA)	Northeastern Alps (NEA)
MAR - EURO4M	C=0.89; RMSE=0.46	C=0.88; RMSE=0.37	0.85; RMSE=0.41
MAR - SPAZM	C=0.87; RMSE=0.26	C=0.85; RMSE=0.45	-
MAR - E-OBS	C=0.84; RMSE=0.69	C=0.86; RMSE=0.83	C=0.79; RMSE=0.90
MAR - HISTALP	C=0.02; RMSE=0.64	C=-0.10; RMSE=0.73	C=-0.22; RMSE=0.66
EURO4M - SPAZM	C=0.99; RMSE=0.38	C=0.97; RMSE=0.62	-
E-OBS - SPAZM	C=0.93; RMSE=0.63	C=0.95; RMSE=1.14	-
E-OBS - EURO4M	C=0.94; RMSE=0.29	C=0.95; RMSE=0.54	C=0.93; RMSE=0.54
EURO4M - HISTALP	C=0.03; RMSE=0.68	C=-0.08; RMSE=0.74	C=-0.26; RMSE=0.67

624

625

626

627

628

629

630

Table 2: Correlation Pearson coefficient computed over 1971-2008 (C) and Root Mean Square Error (RMSE) between the time series of precipitation data over 1971-2008 for the three different subareas described in Figure 1. All the correlations are significant (p -value >0.1), except those computed with the HISTALP data.



631 **Figure captions**

632

633 Figure 1: (a) Annual mean of precipitation (TC, mm year⁻¹) over 1971-2008 in the Alps
634 simulated with the model MAR applied with a resolution of 7km and laterally forced with ERA-
635 20C. The colored boxes correspond to the Southern Alps (SA, orange), the Northwestern Alps
636 (NWA, blue) and the Northeastern Alps (NEA, purple). Precipitation differences (%) between:
637 (b) the MAR experiment and the SPAZM dataset, (c) the MAR experiment and the EURO4M-
638 APGD observational gridded datasets, and the SPAZM and the EURO4M-APGD datasets. (c)
639 and (d) are shown only for the area where the SPAZM data is available. The 1000 m-spaced
640 black contours show the topography in the 7km-resolution model, starting from 500 m.asl and
641 political frontiers are denoted with the black dashed lines. The pattern correlation between MAR
642 outputs and observational data is 0.59 and 0.63 respectively with EURO4M and SPAZM (p-
643 value<1e-200).

644

645 Figure 2: Precipitation (STP) averaged over 1971-2008 simulated by MAR and estimated from
646 reanalyses and observations. (a-b-c-d-e-f) show precipitation as a function of the elevation over
647 the Southern (a) and the Northern (b) French Alps in MAR experiments and SAFRAN
648 reanalysis, and estimated over Switzerland from local meteorological stations and from the MAR
649 grid cells covering Switzerland during summer (c) and winter (d). The vertical gradient averaged
650 over the full domain are shown for winter (e) and summer (f). STP averaged over 1903-2010 in
651 the MAR experiment (shaded, mm.day⁻¹) and observed at MeteoSwiss stations in Switzerland
652 (dots, observations available from the beginning of the XXth century) are shown for summer (g)
653 and winter (h). In (g) and (h), the 1000 m-spaced black contours show the topography with a
654 7km-resolution, starting from 500 m.asl and political frontiers are denoted with the black dashed
655 lines.

656

657 Figure 3: Annual mean precipitation (mm day⁻¹) averaged over the Southern Alps (SA), the
658 Northwestern Alps (NWA) and the Northeastern Alps (NEA) over the period 1971-2008 (top
659 row) and corresponding monthly averaged seasonal cycle over the same period (bottom row).
660 The area covered by the SA, NWA and NEA domains can be visualized in Figure 1. MAR
661 outputs and observational data sets EURO4M, SPAZM, HISTALP and E-OBS are shown (see
662 text for details). E-OBS (orange solid line) is provided with an estimation of the observational
663 uncertainty (orange dashed lines).

664

665 Figure 4: Seasonal linear trends (percent per century) of precipitation over 1903-2010 in winter
666 (a-c), summer (b-d), spring (e) and autumn (f). 1000 m-spaced black contours show the
667 topography in the 7km-resolution model, starting from 500 m.asl and frontiers are denoted with
668 the black dashed lines. In (c-d) and (g-h), the trend is masked when its p-value is below 0.05
669 (level of confidence is lower than 95%; white areas for the model outputs and station data
670 excluded).

671



672 Figure 5: Winter and Summer 1903-2010 trends (percent per century) of WD (a-b), SDII (c-d),
673 MWSD (e-f) and MNWS (g-h) simulated by the MAR model (shaded) and locally observed in
674 Switzerland (dots). WD is computed as a percentage of the available daily data for observations.
675 Any station from the observational network including missing data is excluded when computing
676 the trends.

677

678 Figure 6: Seasonal mean (mm day⁻¹, left) and trends (percent per century, right) over the period
679 1903-2010 of the seasonal Rx1day simulated by MAR (shaded) and locally observed in
680 Switzerland (dots) for Winter (a-b), Spring (c-d), Summer (e-f) and Autumn (g-h).

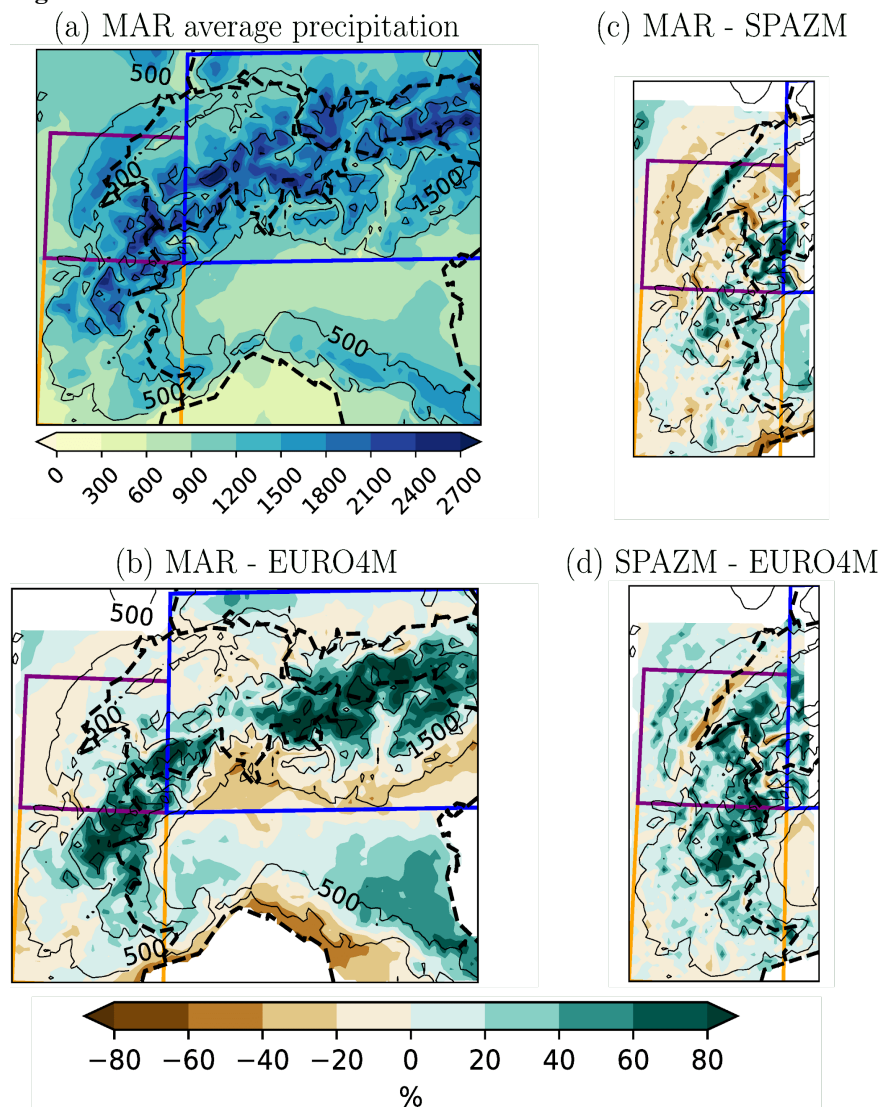
681

682 Figure 7: Mean (a) and maximum (b) of the annual Rx1day and its trend including (c) and
683 excluding (d) the areas where the p-value is lower than 0.05, over 1903-2010. Annual Rx1day
684 (e) and associated p-value of the trend (f) over the same period averaged over the model domain
685 (red for the entire Alpine region and blue for the Swiss domain only) and for the MeteoSwiss
686 network (purple, average of the MeteoSwiss data station available over 1903-2010). The vertical
687 bars in (e) highlight the year before which the p-value never exceeds 0.05.

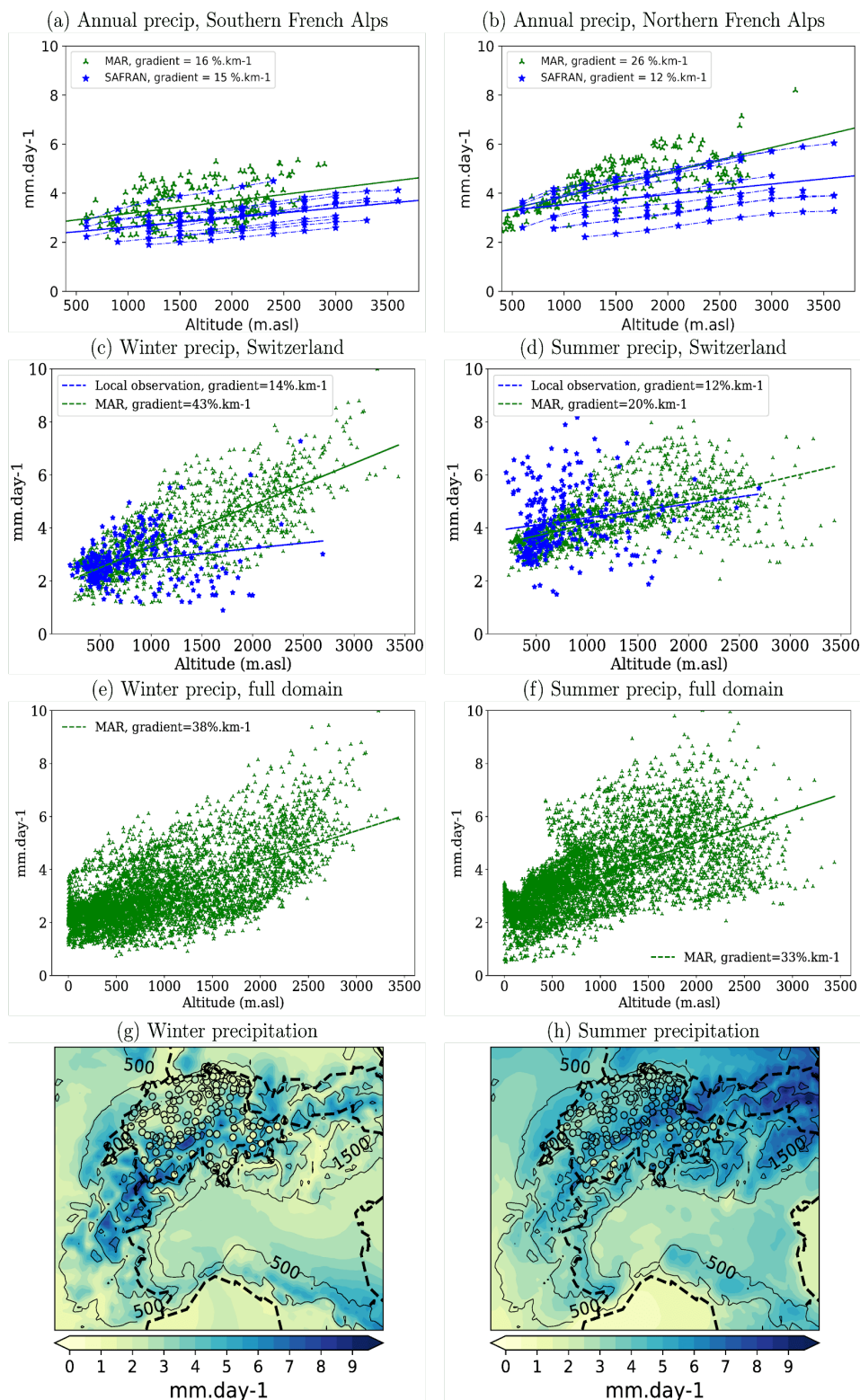
688



689 **Figures:**

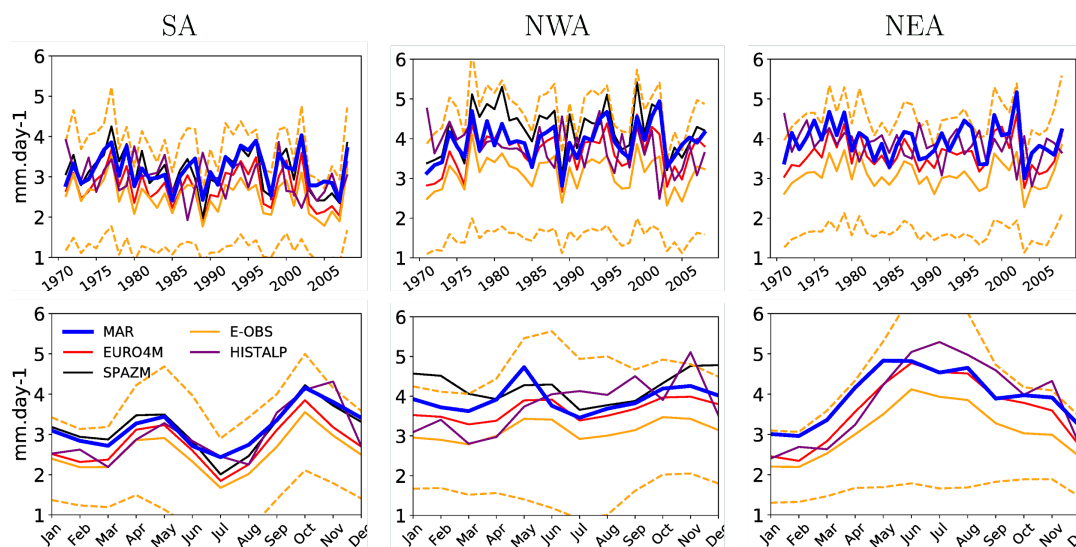


690
691 Figure 1: (a) Annual mean of precipitation (TC, mm year⁻¹) over 1971-2008 in the Alps
692 simulated with the model MAR applied with a resolution of 7km and laterally forced with ERA-
693 20C. The colored boxes correspond to the Southern Alps (SA, orange), the Northwestern Alps
694 (NWA, blue) and the Northeastern Alps (NEA, purple). Precipitation differences (%) between:
695 (b) the MAR experiment and the SPAZM dataset, (c) the MAR experiment and the EURO4M-
696 APGD observational gridded datasets, and the SPAZM and the EURO4M-APGD datasets. (c)
697 and (d) are shown only for the area where the SPAZM data is available. The 1000 m-spaced
698 black contours show the topography in the 7km-resolution model, starting from 500 m.asl and
699 political frontiers are denoted with the black dashed lines. The pattern correlation between MAR
700 outputs and observational data is 0.59 and 0.63 respectively with EURO4M and SPAZM (p-
701 value<1e-200).

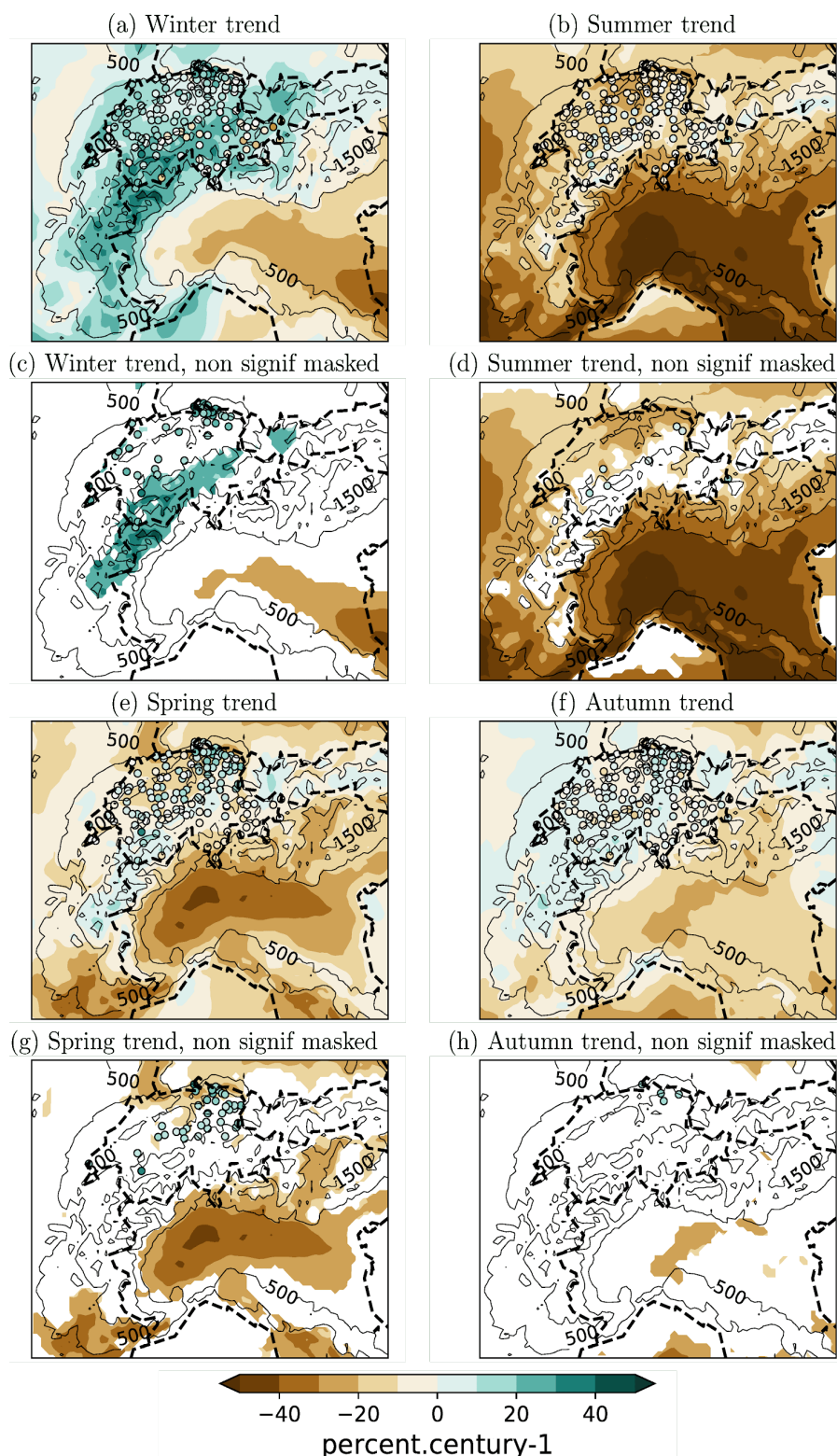




703 Figure 2: Precipitation (STP) averaged over 1971-2008 simulated by MAR and estimated from
 704 reanalyses and observations. (a-b-c-d-e-f) show precipitation as a function of the elevation over
 705 the Southern (a) and the Northern (b) French Alps in MAR experiments and SAFRAN
 706 reanalysis, and estimated over Switzerland from local meteorological stations and from the MAR
 707 grid cells covering Switzerland during summer (c) and winter (d). The vertical gradient averaged
 708 over the full domain are shown for winter (e) and summer (f). STP averaged over 1903-2010 in
 709 the MAR experiment (shaded, mm.day⁻¹) and observed at MeteoSwiss stations in Switzerland
 710 (dots, observations available from the beginning of the XXth century) are shown for summer (g)
 711 and winter (h). In (g) and (h), the 1000 m-spaced black contours show the topography with a
 712 7km-resolution, starting from 500 m.asl and political frontiers are denoted with the black dashed
 713 lines.
 714
 715

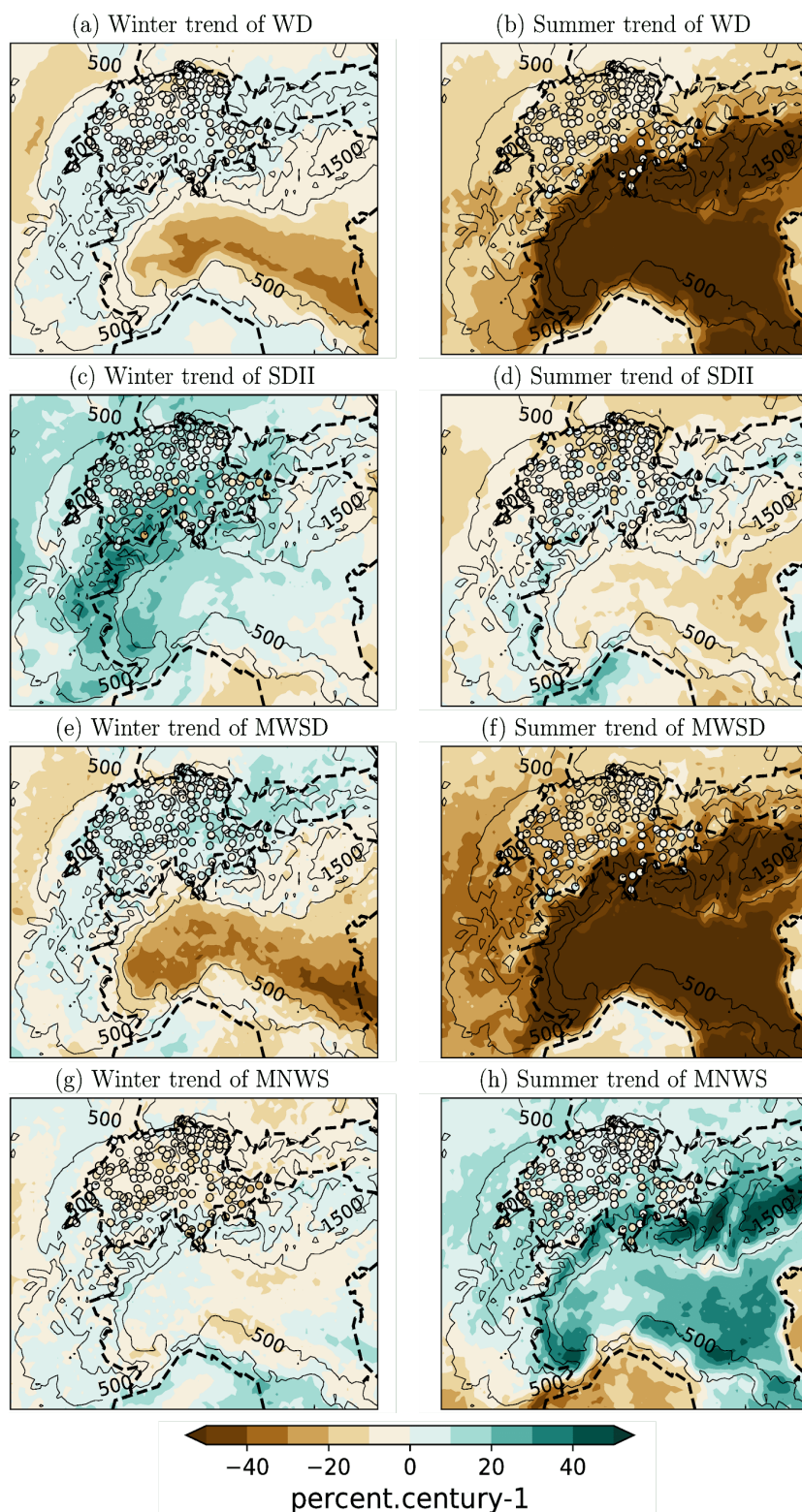


716
 717
 718 Figure 3: Annual mean precipitation (mm day⁻¹) averaged over the Southern Alps (SA), the
 719 Northwestern Alps (NWA) and the Northeastern Alps (NEA) over the period 1971-2008 (top
 720 row) and corresponding monthly averaged seasonal cycle over the same period (bottom row).
 721 The area covered by the SA, NWA and NEA domains can be visualized in Figure 1. MAR
 722 outputs and observational data sets EURO4M, SPAZM, HISTALP and E-OBS are shown (see
 723 text for details). E-OBS (orange solid line) is provided with an estimation of the observational
 724 uncertainty (orange dashed lines).
 725



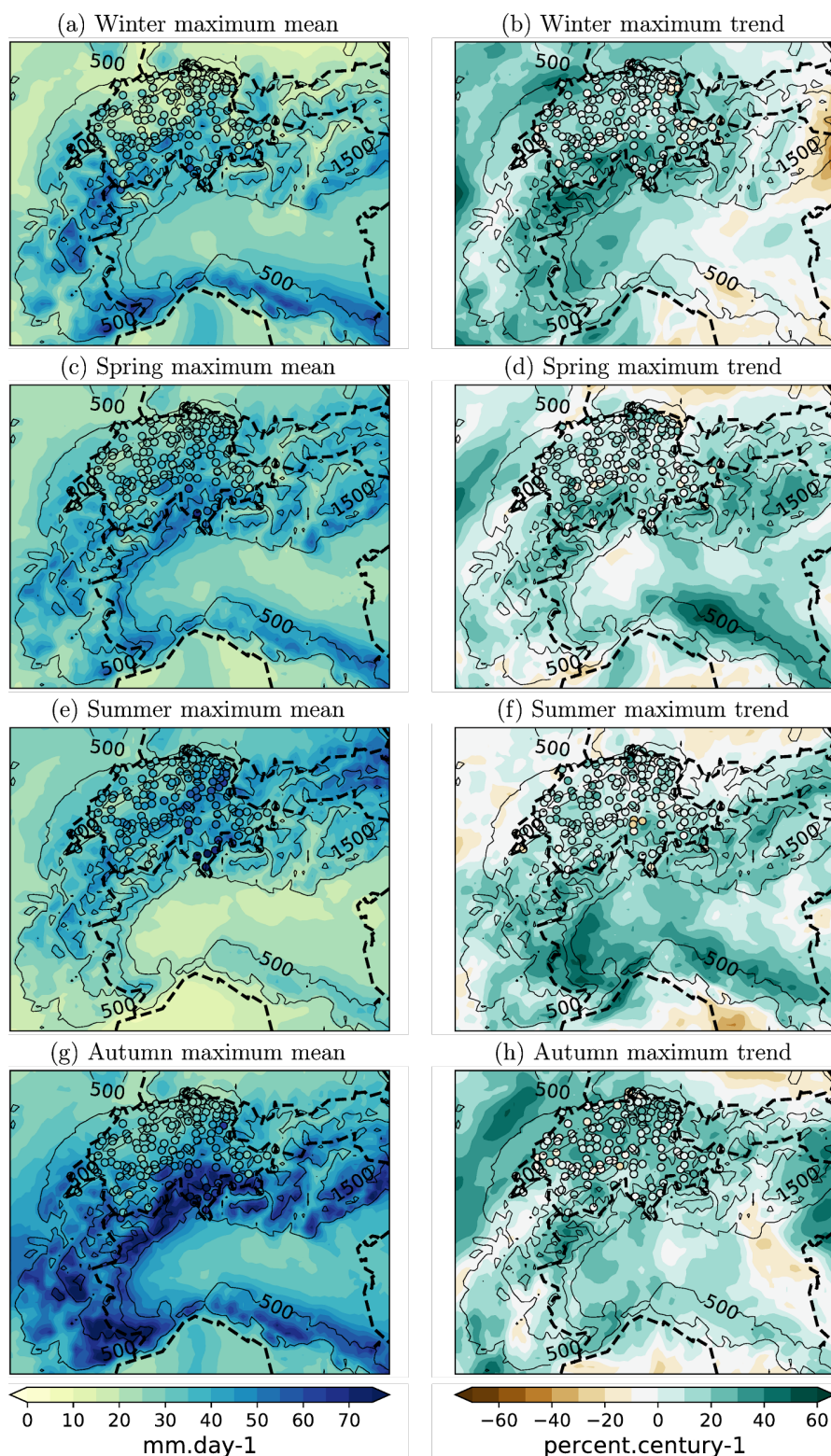


727 Figure 4: Seasonal linear trends (percent per century) of precipitation over 1903-2010 in winter
728 (a-c), summer (b-d), spring (e) and autumn (f). 1000 m-spaced black contours show the
729 topography in the 7km-resolution model, starting from 500 m.asl and frontiers are denoted with
730 the black dashed lines. In (c-d) and (g-h), the trend is masked when its p-value is below 0.05
731 (level of confidence is lower than 95%; white areas for the model outputs and station data
732 excluded).





734 Figure 5: Winter and Summer 1903-2010 trends (percent per century) of WD (a-b), SDII (c-d),
735 MWSD (e-f) and MNWS (g-h) simulated by the MAR model (shaded) and locally observed in
736 Switzerland (dots). WD is computed as a percentage of the available daily data for observations.
737 Any station from the observational network including missing data is excluded when computing
738 the trends.
739

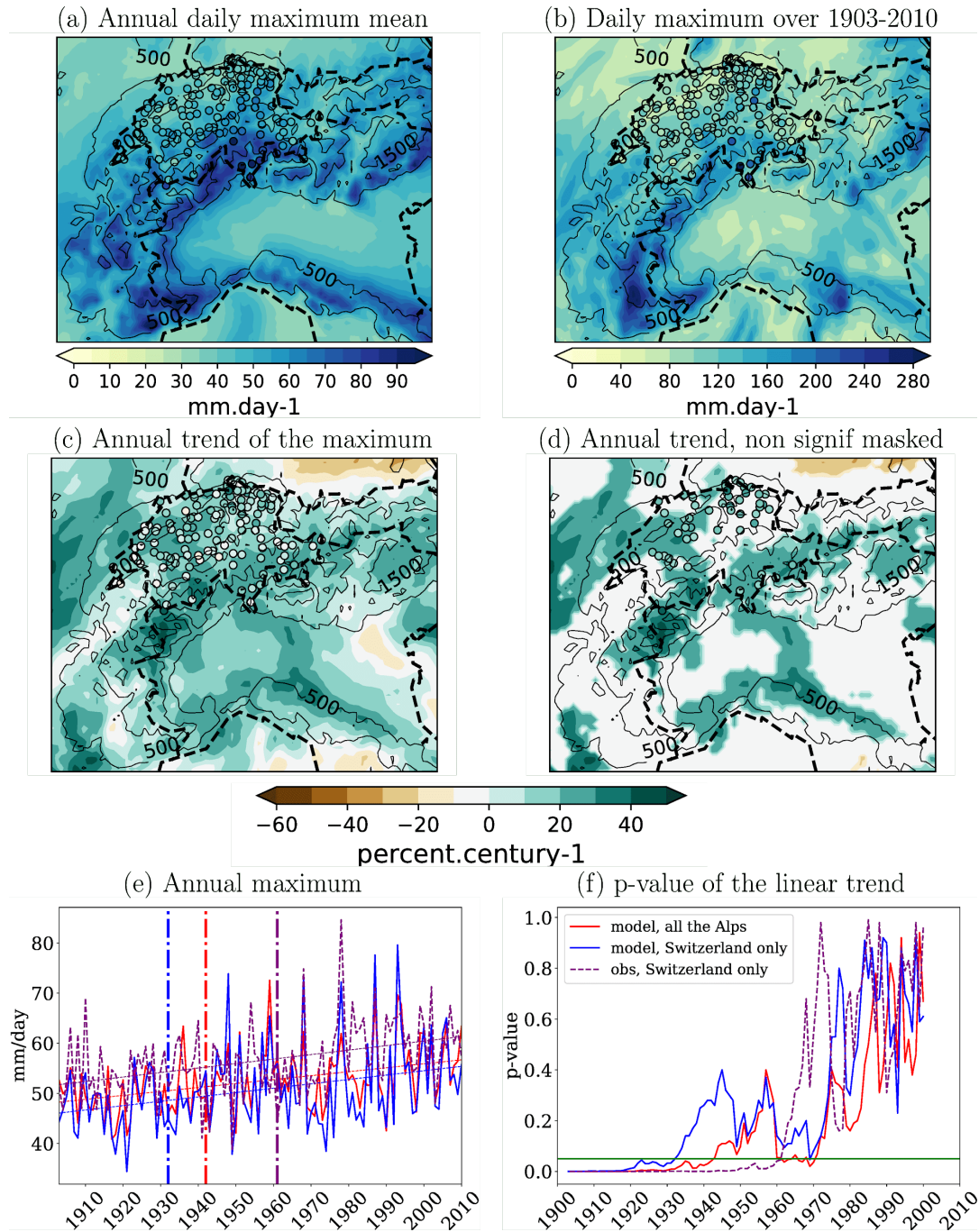




741 Figure 6: Seasonal mean (mm day⁻¹, left) and trends (percent per century, right) over the period
742 1903-2010 of the seasonal Rx1day simulated by MAR (shaded) and locally observed in
743 Switzerland (dots) for Winter (a-b), Spring (c-d), Summer (e-f) and Autumn (g-h).
744



745



746
747



748 Figure 7: Mean (a) and maximum (b) of the annual Rx1day and its trend including (c) and
749 excluding (d) the areas where the p-value is lower than 0.05, over 1903-2010. Annual Rx1day
750 (e) and associated p-value of the trend (f) over the same period averaged over the model domain
751 (red for the entire Alpine region and blue for the Swiss domain only) and for the MeteoSwiss
752 network (purple, average of the MeteoSwiss data station available over 1903-2010). The vertical
753 bars in (e) highlight the year before which the p-value never exceeds 0.05.



754 **References**

755

756 Agosta, C., Amory, C., Kittel, C., Orsi, A., Favier, V., Gallée, H., van den Broeke, M. R.,
757 Lenaerts, J. T. M., van Wessem, J. M., van de Berg, W. J., and Fettweis, X.: Estimation of the
758 Antarctic surface mass balance using the regional climate model MAR (1979–2015) and
759 identification of dominant processes, *The Cryosphere*, 13, 281–296, [https://doi.org/10.5194/tc-](https://doi.org/10.5194/tc-13-281-2019)
760 13-281-2019, 2019.

761 Amory, C., Trouvilliez, A., Gallée, H., Favier, V., Naaim-Bouvet, F., Genthon, C., Agosta, C.,
762 Piard, L., and Bellot, H.: Comparison between observed and simulated aeolian snow mass
763 fluxes in Adélie Land, East Antarctica, *The Cryosphere*, 9, 1373–1383,
764 <https://doi.org/10.5194/tc-9-1373-2015>, 2015.

765 Auer, I., Böhm, R., Jurkovic, A., Lipa, W., Orlik, A., Potzmann, R., Schöner, W., Ungersböck,
766 M., Matulla, C., Briffa, K. and Jones, P.: HISTALP—historical instrumental climatological
767 surface time series of the Greater Alpine Region. *International Journal of Climatology: A*
768 *Journal of the Royal Meteorological Society*, 27(1), pp.17-46, 2007.

769 Auer, I., and R. Böhm: Combined temperature-precipitation variations in Austria during the
770 instrumental period, *Theoretical and applied climatology* 49, no. 3 (1994): 161-174, 1994.

771 Ban, N., J. Schmidli and Schär, C.: Evaluation of the convection-resolving regional climate
772 modeling approach in decade-long simulations, *J. Geophys. Res. Atmos.*, 119, 7889–7907,
773 doi:10.1002/2014JD021478, 2014.

774 Ban, N., Schmidli, J. and Schär, C.: Heavy precipitation in a changing climate: Does short-term
775 summer precipitation increase faster?. *Geophysical Research Letters*, 42(4), pp.1165-1172,
776 2015.

777 Bartolini, E., Claps, P., and D'Odorico, P.: Interannual variability of winter precipitation in the
778 European Alps: relations with the North Atlantic Oscillation., *Hydrol. Earth Syst. Sci.*, 13, 17–
779 25, <https://doi.org/10.5194/hess-13-17-2009>, 2009.

780 Bechtold, P., Basile, E., Guichard, F., Mascart, P., and Richard, E.: A mass flux convection
781 scheme for regional and global models, *Q. J. Roy. Meteorol. Soc.*, 127, 869–886, 2001.

782 Beniston, M., Farinotti, D., Stoffel, M., Andreassen, L. M., Coppola, E., Eckert, N., Fantini, A.,
783 Giacona, F., Hauck, C., Huss, M., Huwald, H., Lehning, M., López-Moreno, J.-I., Magnusson,
784 J., Marty, C., Morán-Tejedá, E., Morin, S., Naaim, M., Provenzale, A., Rabatel, A., Six, D.,
785 Stötter, J., Strasser, U., Terzago, S., and Vincent, C.: The European mountain cryosphere: a
786 review of its current state, trends, and future challenges, *The Cryosphere*, 12, 759–794,
787 <https://doi.org/10.5194/tc-12-759-2018>, 2018.

788 Beniston, M.: Mountain weather and climate: a general overview and a focus on climatic change
789 in the Alps. *Hydrobiologia*, 562(1), pp.3-16, 2006.

790 Brogli, R., Kröner, N., Sørland, S.L., Lüthi, D. and Schär, C.: The Role of Hadley Circulation
791 and Lapse-Rate Changes for the Future European Summer Climate. *Journal of Climate*, 32(2),
792 pp.385-404, <https://doi.org/10.1175/JCLI-D-18-0431.1>, 2019.



- 793 Brönnimann, S., Rajczak, J., Fischer, E. M., Raible, C. C., Rohrer, M., and Schär, C.: Changing
794 seasonality of moderate and extreme precipitation events in the Alps, *Nat. Hazards Earth Syst.*
795 *Sci.*, 18, 2047–2056, <https://doi.org/10.5194/nhess-18-2047-2018>, 2018.
- 796 Brugnara, Y. and Maugeri, M.: Daily precipitation variability in the southern Alps since the late
797 19th century. *International journal of climatology*, <https://doi.org/10.1002/joc.6034>, 2019.
- 798 Brunetti, M., Lentini, G., Maugeri, M., Nanni, T., Auer, I., Boehm, R. and Schoener, W.:
799 Climate variability and change in the Greater Alpine Region over the last two centuries based
800 on multi-variable analysis. *International Journal of Climatology: A Journal of the Royal*
801 *Meteorological Society*, 29(15), pp.2197-2225, 2009.
- 802 Brunetti, M., Maugeri, M., Nanni, T., Auer, I., Böhm, R. and Schöner, W.: Precipitation
803 variability and changes in the greater Alpine region over the 1800–2003 period. *Journal of*
804 *Geophysical Research: Atmospheres*, 111(D11), <https://doi.org/10.1029/2005JD006674>, 2006.
- 805 Cornes, R., G. van der Schrier, E.J.M. van den Besselaar, and Jones, P.D.: An Ensemble Version
806 of the E-OBS Temperature and Precipitation Datasets, *J. Geophys. Res. Atmos.*, 123.
807 doi:10.1029/2017JD028200, 2018.
- 808 Dee, D.P., Uppala, S.M., Simmons, A.J., Berrisford, P., Poli, P., Kobayashi, S., Andrae, U.,
809 Balmaseda, M.A., Balsamo, G., Bauer, D.P. and Bechtold, P.: The ERA-Interim reanalysis:
810 Configuration and performance of the data assimilation system. *Quarterly Journal of the royal*
811 *meteorological society*, 137(656), pp.553-597, 2011.
- 812 De Ridder, K. and Schayes, G.: The IAGL land surface model, *J. Appl. Meteorol.*, 36, 167–183,
813 1997.
- 814 Doutreloup, S., Wyard, C., Amory, C., Kittel, C., Erpicum, M. and Fettweis, X.: Sensitivity to
815 Convective Schemes on Precipitation Simulated by the Regional Climate Model MAR over
816 Belgium (1987–2017). *Atmosphere*, 10(1), p.34, 2019.
- 817 Douville, H. and Plazzotta, M.: Midlatitude summer drying: An underestimated threat in CMIP5
818 models?. *Geophysical Research Letters*, 44(19), pp.9967-9975, 2017
- 819 Durand, Y., Laternser, M., Giraud, G., Etchevers, P., Lesaffre, B. and Mérindol, L.: Reanalysis
820 of 44 yr of climate in the French Alps (1958–2002): methodology, model validation,
821 climatology, and trends for air temperature and precipitation. *Journal of Applied Meteorology*
822 *and Climatology*, 48(3), pp.429-449, 2009.
- 823 Efthymiadis, D., Jones, P.D., Briffa, K.R., Böhm, R. and Maugeri, M.: Influence of large-scale
824 atmospheric circulation on climate variability in the Greater Alpine Region of Europe. *Journal*
825 *of Geophysical Research: Atmospheres*, 112(D12), 2007.
- 826 Evin G., Wilhelm B., Jenny J.P.: Flood hazard assessment of the Rhône River revisited with
827 reconstructed discharges from lake sediments, *Global and Planetary Change* 172, 114-123,
828 2019.



- 829 Picouet, C.: Réanalyse de l'équivalent en eau de la couverture neigeuse : développement d'un
830 modèle de neige au pixel. Partie 2 : Structuration d'un modèle neige à l'échelle du pixel au droit
831 des chroniques historiques SWE. Rapport Technique EDF-LTHE-Alcofra, 2012.
- 832 Fantini, A., Raffaele, F., Torma, C., Bacer, S., Coppola, E., Giorgi, F., Ahrens, B., Dubois, C.,
833 Sanchez, E. and Verdecchia, M.: Assessment of multiple daily precipitation statistics in ERA-
834 Interim driven Med-CORDEX and EURO-CORDEX experiments against high resolution
835 observations. *Climate dynamics*, 51(3), pp.877-900, 2018.
- 836 Fettweis, X., Box, J. E., Agosta, C., Amory, C., Kittel, C., Lang, C., van As, D., Machguth, H.,
837 and Gallée, H.: Reconstructions of the 1900–2015 Greenland ice sheet surface mass balance
838 using the regional climate MAR model, *The Cryosphere*, 11, 1015–1033,
839 <https://doi.org/10.5194/tc-11-1015-2017>, 2017.
- 840 Frei, C., and F. Isotta: Ensemble spatial precipitation analysis from rain gauge data -
841 Methodology and application in the European Alps. *J. Geophys. Res. Atmos.*, 124, 5757–
842 5778, <https://doi.org/10.1029/2018JD030004>, 2019.
- 843 Giorgi, F., Torma, C., Coppola, E., Ban, N., Schär, C. and Somot, S.: Enhanced summer
844 convective rainfall at Alpine high elevations in response to climate warming. *Nature*
845 *Geoscience*, 9(8), p.584, 2016.
- 846 Giorgi, F. and Lionello, P.: Climate change projections for the Mediterranean region. *Global and*
847 *planetary change*, 63(2-3), pp.90-104, 2008.
- 848 Gobiet, A., Kotlarski, S., Beniston, M., Heinrich, G., Rajczak, J. and Stoffel, M.: 21st century
849 climate change in the European Alps—a review. *Science of the Total Environment*, 493,
850 pp.1138-1151, 2014.
- 851 Gallée, H., Pettré, P. and Schayes, G.: Sudden cessation of katabatic winds in Adélie Land,
852 Antarctica. *Journal of Applied Meteorology*, 35(7), pp.1142-1152, 1996.
- 853 Gallée, H.: Simulation of the mesocyclonic activity in the Ross Sea, Antarctica, *Mon. Weather*
854 *Rev.*, 123, 2051–2069, 1995.
- 855 Gallée, H. and Schayes, G.: Development of a three-dimensional meso-gamma primitive
856 equation model: katabatic winds simulation in the area of Terra Nova bay, Antarctica, *Mon.*
857 *Weather. Rev.*, 122, 671–685, 1994.
- 858 Gallée, H., Guyomarch, G., and Brun, E.: Impact of snowdrift on the Antarctic ice sheet surface
859 mass balance: possible sensitivity to snow-surface properties, *Bound.-Lay. Meteorol.*, 99, 1–19,
860 2001.
- 861 Gallée, H., Moufouma-Okia, W., Bechtold, P., Brasseur, O., Dupays, I., Marbaix, P., Messenger,
862 C., Ramel, R., and Lebel, T.: A high resolution simulation of a West African rainy season using
863 a regional climate model, *J. Geophys. Res.*, 109, D05108, doi:10.1029/2003JD004020, 2004.
- 864 Gallée, H., Peyaud, V., and Goodwin. I.: Simulation of the net snow accumulation along the
865 Wilkes Land transect, Antarctica, with a regional climate model, *Ann. Glaciol.*, 41, 17–22,
866 2005.



- 867 Gallée, H., Trouvilliez, A., Agosta, C., Genthon, C., Favier, V. and Naaim-Bouvet, F.: Transport
868 of snow by the wind: A comparison between observations in Adélie Land, Antarctica, and
869 simulations made with the regional climate model MAR. *Boundary-layer meteorology*, 146(1),
870 pp.133-147, 2013.
- 871 Gottardi, F.: Estimation statistique et réanalyse des précipitations en montagne Utilisation
872 d'ébauches par types de temps et assimilation de données d'enneigement Application aux grands
873 massifs montagneux français, PhD report, University Joseph Fourier and INPG,
874 <https://tel.archives-ouvertes.fr/tel-00419170>, 2009.
- 875 Gouttevin, I., Turko, M., Branger, F., Leblois, E., Sicart, J.E., Amélioration de la modélisation
876 hydrologique distribuée en conditions naturelles dans les Alpes, Internal report, Action Neige
877 2016-2017.
- 878 Guillod, B. P., Jones, R. G., Bowery, A., Haustein, K., Massey, N. R., Mitchell, D. M., Otto, F.
879 E. L., Sparrow, S. N., Uhe, P., Wallom, D. C. H., Wilson, S., and Allen, M. R.: *weather@home*
880 2: validation of an improved global–regional climate modelling system, *Geosci. Model Dev.*,
881 10, 1849-1872, <https://doi.org/10.5194/gmd-10-1849-2017>, 2017.
- 882 Hersbach, H. and Dee, D.: ERA5 reanalysis is in production, ECMWF Newsletter 147,
883 ECMWF. Reading, UK, 2016.
- 884 Hock, R., G. Rasul, C. Adler, B. Cáceres, S. Gruber, Y. Hirabayashi, M. Jackson, A. Kääb, S.
885 Kang, S. Kutuzov, Al. Milner, U. Molau, S. Morin, B. Orlove, and H. Steltzer, 2019: High
886 Mountain Areas. In : IPCC Special Report on the Ocean and Cryosphere in a Changing Climate
887 [H.-O. Pörtner, D.C. Roberts, V. Masson-Delmotte, P. Zhai, M. Tignor, E. Poloczanska K.
888 Mintenbeck, A. Alegría, M. Nicolai, A. Okem, J. Petzold, B. Rama, N.M. Weyer (eds.)]. In
889 press. http://report.ipcc.ch/srocc/pdf/SROCC_FinalDraft_Chapter2.pdf, in press.
- 890 Hoerling, M., Eischeid, J., Perlwitz, J., Quan, X., Zhang, T. and Pegion, P.: On the increased
891 frequency of Mediterranean drought. *Journal of Climate*, 25(6), pp.2146-2161, 2012.
- 892 Isotta, F.A., Frei, C., Weilguni, V., Perčec Tadić, M., Lassegues, P., Rudolf, B., Pavan, V.,
893 Cacciamani, C., Antolini, G., Ratto, S.M. and Munari, M.: The climate of daily precipitation in
894 the Alps: development and analysis of a high-resolution grid dataset from pan-Alpine rain
895 gauge data. *International Journal of Climatology*, 34(5), pp.1657-1675, 2014.
- 896 Keiler, M., Knight, J. and Harrison, S.: Climate change and geomorphological hazards in the
897 eastern European Alps. *Philosophical Transactions of the Royal Society A: Mathematical,*
898 *Physical and Engineering Sciences*, 368(1919), pp.2461-2479, 2010.
- 899 Koch, D., Bauer, S.E., Del Genio, A., Faluvegi, G., McConnell, J.R., Menon, S., Miller, R.L.,
900 Rind, D., Ruedy, R., Schmidt, G.A. and Shindell, D.: Coupled aerosol-chemistry–climate
901 twentieth-century transient model investigation: trends in short-lived species and climate
902 responses. *Journal of Climate*, 24(11), pp.2693-2714, 2011.
- 903 Kochendorfer, J., Rasmussen, R., Wolff, M., Baker, B., Hall, M. E., Meyers, T., Landolt, S.,
904 Jachcik, A., Isaksen, K., Brækkan, R., and Leeper, R.: The quantification and correction of



- 905 wind-induced precipitation measurement errors, *Hydrol. Earth Syst. Sci.*, 21, 1973-1989,
906 <https://doi.org/10.5194/hess-21-1973-2017>, 2017.
- 907 Kuglitsch, F.G., Toreti, A., Xoplaki, E., Della Marta, P.M., Zerefos, C.S., Türkeş, M. and
908 Luterbacher, J.: Heat wave changes in the eastern Mediterranean since 1960. *Geophysical*
909 *Research Letters*, 37(4), <https://doi.org/10.1029/2009GL041841>, 2010.
- 910 Lüthi, S., Ban, N., Kotlarski, S., Steger, C.R., Jonas, T. and Schär, C.: Projections of Alpine
911 Snow-Cover in a High-Resolution Climate Simulation. *Atmosphere*, 10(8), p.463, 2019.
- 912 Dell'Aquila, A., Mariotti, A., Bastin, S., Calmanti, S., Cavicchia, L., Deque, M., Djurdjevic, V.,
913 Dominguez, M., Gaertner, M. and Gualdi, S.: Evaluation of simulated decadal variations over
914 the Euro-Mediterranean region from ENSEMBLES to Med-CORDEX. *Climate dynamics*,
915 51(3), pp.857-876, 2018.
- 916 Mariotti, A., Pan, Y., Zeng, N. and Alessandri, A.: Long-term climate change in the
917 Mediterranean region in the midst of decadal variability. *Climate Dynamics*, 44(5-6), pp.1437-
918 1456, 2015.
- 919 Masson, D. and Frei, C.: Spatial analysis of precipitation in a high-mountain region: exploring
920 methods with multi-scale topographic predictors and circulation types. *Hydrology and Earth*
921 *System Sciences*, 18(11), pp.4543-4563, 2014.
- 922 Masson, D. and Frei, C.: Long-term variations and trends of mesoscale precipitation in the
923 Alps: recalculation and update for 1901–2008. *International Journal of Climatology*, 36(1),
924 pp.492-500, 2016.
- 925 Messenger, C., Gallée, H., and Brasseur, O.: Precipitation sensitivity to regional SST in a regional
926 climate simulation during the West African monsoon for two dry years, *Clim. Dynam.*, 22,
927 249–266, doi:10.1007/s00382-003-0381-x, 2004.
- 928 Messenger, C., Gallée, H., Brasseur, O., Cappelaere, B., Peugeot, C., Séguis, L., Vauclin, M.,
929 Ramel, R., Grasseau, G., Léger, L., Girou, D: Influence of observed and RCM-simulated
930 precipitation on the water discharge over the Sirba basin, Burkina Faso/Niger. *Climate*
931 *Dynamics*, 27 (2-3), pp. 199-214, DOI: 10.1007/s00382-006-0131-y, 2006.
- 932 Morcrette, J.-J. Assessment of the ECMWF Model Cloudiness and Surface Radiation Fields at
933 the ARM SGP Site. *Mon. Weather Rev.* 2002, 130, 257–277.
- 934 Naithani, J., Gallée, H. and Schayes, G.: Marine air intrusion into the Adelie Land sector of East
935 Antarctica: A study using the regional climate model (MAR). *Journal of Geophysical Research:*
936 *Atmospheres*, 107(D11), pp.ACL-6, 2002.
- 937 Napoli, A., Crespi, A., Ragone, F., Maugeri, M. and Pasquero, C.: Variability of orographic
938 enhancement of precipitation in the Alpine region. *Scientific reports*, 9(1), pp.1-8, 2019.
- 939 Peterson, T.C., and Coauthors: Report on the Activities of the Working Group on Climate
940 Change Detection and Related Rapporteurs 1998-2001,
941 http://etccdi.pacificclimate.org/list_27_indices.shtml, WMO, Rep. WCDMP-47, WMO-TD
942 1071, Geneve, Switzerland, 143pp, 2001.



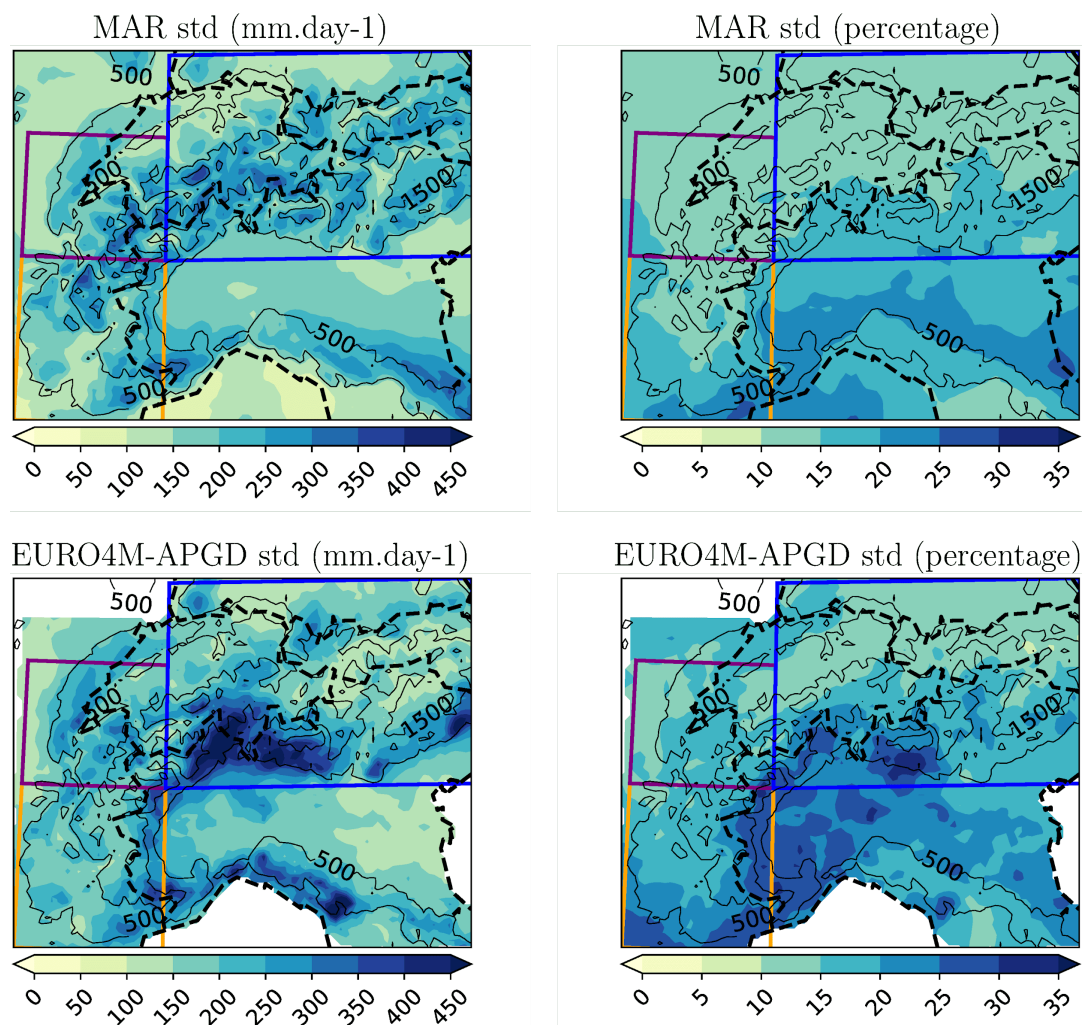
- 943 Picouet, C., Réanalyse de l'équivalent en eau de la couverture neigeuse : développement d'un
944 modèle de neige au pixel. Partie 2 : Structuration d'un modèle neige à l'échelle du pixel au droit
945 des chroniques historiques SWE. Technical report EDF-LTHE-Alcotra, 2012.
- 946 Pieri, A.B., von Hardenberg, J., Parodi, A. and Provenzale, A.: Sensitivity of precipitation
947 statistics to resolution, microphysics, and convective parameterization: A case study with the
948 high-resolution WRF climate model over Europe. *Journal of Hydrometeorology*, 16(4),
949 pp.1857-1872, 2015.
- 950 Poli, P., Hersbach, H., Dee, D.P., Berrisford, P., Simmons, A.J., Vitart, F., Laloyaux, P., Tan,
951 D.G., Peubey, C., Thépaut, J.N. and Trémolet, Y.: ERA-20C: An atmospheric reanalysis of the
952 twentieth century. *Journal of Climate*, 29(11), pp.4083-4097, 2016.
- 953 Qasmi, S., Cassou, C., & Boé, J.: Teleconnection between Atlantic multidecadal variability and
954 European temperature: Diversity and evaluation of the Coupled Model Intercomparison Project
955 phase 5 models. *Geophysical Research Letters*, 44(21), 11-140, 2017.
- 956 Schmidli, J., Schmutz, C., Frei, C., Wanner, H. and Schär, C.: Mesoscale precipitation variability
957 in the region of the European Alps during the 20th century. *International Journal of*
958 *Climatology: A Journal of the Royal Meteorological Society*, 22(9), pp.1049-1074, 2002.
- 959 Schmidli, J. and Frei, C.: Trends of heavy precipitation and wet and dry spells in Switzerland
960 during the 20th century. *International Journal of Climatology: A Journal of the Royal*
961 *Meteorological Society*, 25(6), pp.753-771, 2005.
- 962 Smiatek, G., Kunstmann, H. and Senatore, A.: EURO-CORDEX regional climate model
963 analysis for the Greater Alpine Region: Performance and expected future change. *Journal of*
964 *Geophysical Research: Atmospheres*, 121(13), pp.7710-7728, 2016.
- 965 Steger, C., Kotlarski, S., Jonas, T., and Schär, C.: Alpine snow cover in a changing climate: A
966 regional climate model perspective, *Clim. Dynam.*, 41, 735–754, 2013
- 967 Torma, C., Giorgi, F. and Coppola, E.: Added value of regional climate modeling over areas
968 characterized by complex terrain—Precipitation over the Alps. *Journal of Geophysical*
969 *Research: Atmospheres*, 120(9), pp.3957-3972, 2015.
- 970 Uppala, S.M., Kållberg, P.W., Simmons, A.J., Andrae, U., Bechtold, V.D.C., Fiorino, M.,
971 Gibson, J.K., Haseler, J., Hernandez, A., Kelly, G.A. and Li, X.: The ERA-40 re-analysis.
972 *Quarterly Journal of the Royal Meteorological Society: A journal of the atmospheric sciences,*
973 *applied meteorology and physical oceanography*, 131(612), pp.2961-3012, 2005.
- 974 Van den Besselaar, E.J., Haylock, M.R., Van der Schrier, G. and Klein Tank, A.M.G.: A
975 European daily high-resolution observational gridded data set of sea level pressure. *Journal of*
976 *Geophysical Research: Atmospheres*, 116(D11), 2011.
- 977 Verfaillie, D., Favier, V., Gallée, H., Fettweis, X, Agosta, C., Jomelli, V. Regional modeling of
978 surface mass balance on the Cook Ice Cap, Kerguelen Islands, *Climate Dynamics*, DOI:
979 10.1007/s00382-019-04904-z., 2019.



- 980 Vionnet, V., Six, D., Auger, L., Dumont, M., Lafaysse, M., Quéno, L., Réveillet, M.,
981 Dombrowski Etchevers, I., Thibert, E. and Vincent, C., Sub-kilometer precipitation datasets for
982 snowpack and glacier modeling in alpine terrain, *Frontiers in Earth Science*, 7, p.182., 2019.
- 983 Viviroli, D. and Weingartner, R.: “Water towers”—A global view of the hydrological
984 importance of mountains. In *Mountains: sources of water, sources of knowledge* (pp. 15-20).
985 Springer, Dordrecht, 2008.
- 986 Viviroli, D., Kummu, M., Meybeck, M. and Wada, Y.: Increasing dependence of lowland
987 population on mountain water resources, <https://eartharxiv.org/fr5uj>, 2019.
- 988 Wanner, H., Rickli, R., Salvisberg, E., Schmutz, C. and Schüepp, M.: Global climate change and
989 variability and its influence on alpine climate—concepts and observations. *Theoretical and
990 Applied Climatology*, 58(3-4), pp.221-243, 1997.
- 991 Wyard, C., Doutreloup, S., Belleflamme, A., Wild, M. and Fettweis, X.: Global Radiative Flux
992 and Cloudiness Variability for the Period 1959–2010 in Belgium: A Comparison between
993 Reanalyses and the Regional Climate Model MAR. *Atmosphere*, 9(7), p.262, 2018.
- 994 Wyard, C., Scholzen, C., Fettweis, X., Van Campenhout, J. and François, L., 2017. Decrease in
995 climatic conditions favouring floods in the south-east of Belgium over 1959–2010 using the
996 regional climate model MAR. *International Journal of Climatology*, 37(5), pp.2782-2796, 2017.
- 997 Zubler, E.M., Fischer, A.M., Fröb, F. and Liniger, M.A.: Climate change signals of CMIP5
998 general circulation models over the Alps—impact of model selection. *International Journal of
999 Climatology*, 36(8), pp.3088-3104, 2016.
- 1000
1001
1002



1003 Appendix
1004



1005
1006
1007
1008
1009

Figure A1: Standard deviation of annual precipitation over 1971-2008, in mm.day-1 (left) and in percent (right), in the MAR experiment (top) and in the EURO4M-APGD dataset (bottom).